Response of the Equatorial Thermocline to Extratropical Buoyancy Forcing

SANG-IK SHIN AND ZHENGYU LIU

Center for Climatic Research and Department of Atmospheric and Oceanic Sciences, University of Wisconsin—Madison, Madison, Wisconsin

(Manuscript received 22 April 1999, in final form 7 January 2000)

ABSTRACT

The GFDL Modular Ocean Model and the Miami Isopycnal Ocean Model are used to investigate the response of the equatorial thermocline to extratropical buoyancy forcing. Passive tracers and analytical theories are also used to shed light on the dynamics of the thermocline response. The major findings are the following. (i) The midlatitude region seems to be the optimal region for surface buoyancy forcing to affect the equatorial thermocline. This occurs because, first, thermocline anomalies in the midlatitudes can penetrate into the equator very efficiently; second, buoyancy forcing generates a strong local response in the midlatitudes. (ii) Dynamic waves as well as thermocline ventilation contribute to the response in the equatorial thermocline. Consequently, equatorward penetration is substantially greater for a temperature anomaly than for a passive tracer. (iii) Midlatitude forcing generates a significant temperature response in the equatorial thermocline for forcing periods longer than decadal. (iv) For a low latitude (10°–20°) buoyancy forcing, the equatorial thermocline could be dominated by a temperature anomaly that has the opposite sign to the surface forcing because of the strong higher mode baroclinic response in the ventilated thermocline. Finally, the relevance of this work to observations and climate variability is also discussed.

1. Introduction

Despite the important role of the equatorial thermocline in long term climate change (Gu and Philander 1997; Cane et al. 1997; Zhang et al. 1998), the mechanism for the maintenance of the equatorial thermocline remains poorly understood. In principle, the equatorial thermocline is controlled either by high-latitude buoyancy forcing through the deep thermohaline circulation or by extratropical wind and buoyancy forcing through the shallow thermocline ventilation. Here, we are concerned with the latter process. We are particularly interested in the effect of extratropical buoyancy forcing because this effect has been studied the least.

Early studies on the effect of buoyancy forcing on the permanent thermocline have focused on the local response in the extratropics (Magaard 1977). At annual or shorter timescales, local responses to midlatitude buoyancy forcing seem to be weak relative to the wind stress forcing (Frankignoul and Muller 1979). Recent studies suggest that, with the aid of nonlocal ventilation processes, surface buoyancy forcing may induce significant thermocline variability in the subtropics at decadal or longer timescales (Liu and Pedlosky 1994; Liu 1999; Schneider et al. 1999; Huang and Pedlosky 1999). While these studies focused on the extratropics, the remote response of the equatorial thermocline to extratropical buoyancy forcing remains poorly understood. In what region, and at what timescales, do extratropical buoyancy forcing affect the equatorial thermocline most significantly? How strong is the response of the equatorial thermocline? Is the equatorial temperature response always the same sign as the extratropical surface forcing, as one would expect for a passive tracer?

Here a systematic investigation is attempted to understand the response of the equatorial thermocline to extratropical buoyancy forcing in two ocean general circulation models (OGCM): the GFDL MOM2 (Pacanowaski 1996) and the Miami Isopycnal Model (MICOM) (Bleck et al. 1992). Extensive experiments suggest that, at interdecadal or longer timescales, the midlatitude is the region where surface buoyancy forcing affects the equatorial thermocline most efficiently. Furthermore, the equatorial response is induced by not only subduction flow, but also dynamic waves. Finally, for buoyancy forcing at low latitude, the sign of the dominant equatorial thermocline response could be the opposite to the surface forcing due to strong higher mode baroclinic response. This paper is arranged as follows. Section 2 introduces the models and experiments, and we will focus on the MOM2 experiments first. Section 3 discusses the optimal latitude region for extratropical buoyancy forcing to affect the equatorial thermocline.

Corresponding author address: Z. Liu, Department of Atmospheric and Oceanic Sciences, University of Wisconsin—Madison, 1225 W. Dayton St., Madison, WI 53706.
E-mail: zliu3@facstaff.wisc.edu

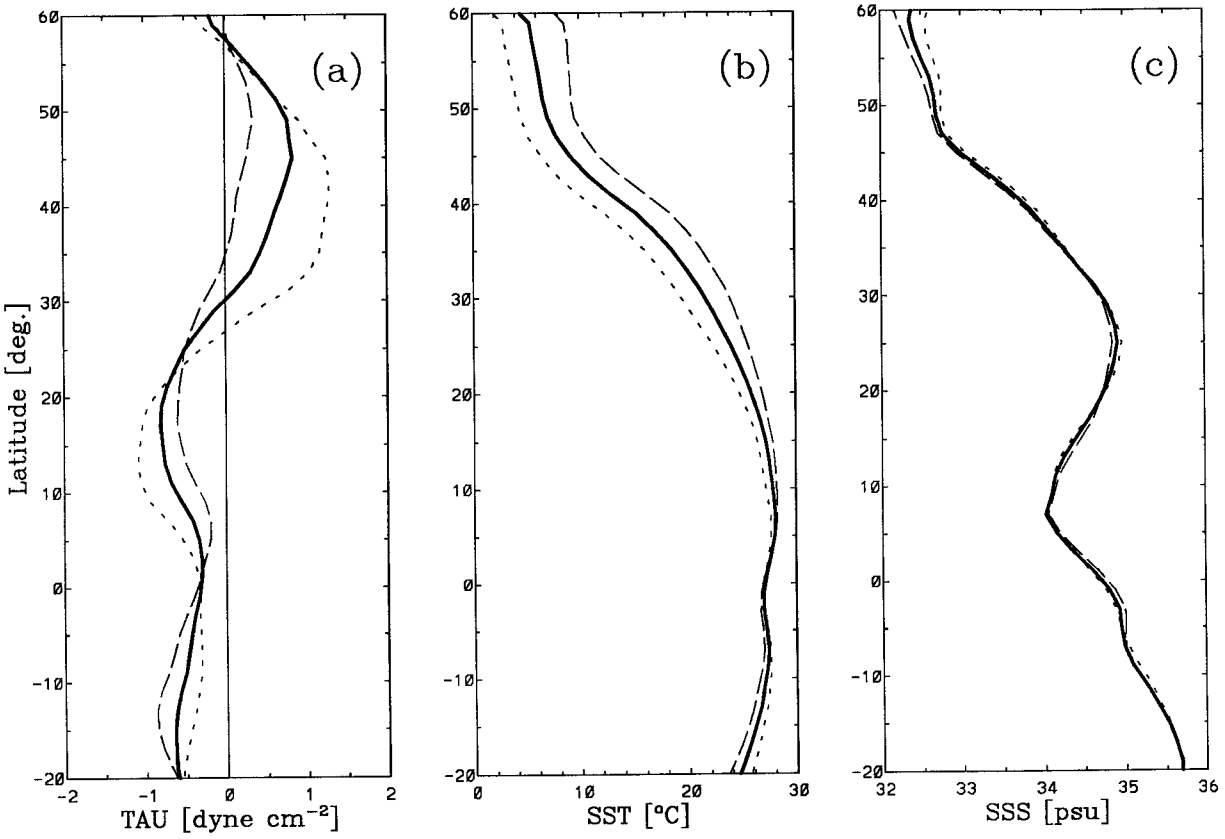

FIG. 1. Latitudinal profiles of model forcing: (a) wind stress, (b) SST, and (c) SSS. Dash, dot, and solid lines represent summer, winter, and annual mean, respectively.

In section 4, we study the response to forcing of different timescales. Section 5 discusses the MICOM experiments and reexamine the equatorial response to low latitude forcing. A summary and discussions are given in section 6. An analytical study on the response of the ventilated thermocline to surface buoyancy forcing is given in the appendix.

2. Model and experiments

Extensive experiments are performed to assure the robustness of our conclusions. This was deemed necessary because of the lack of a systematic study so far on the maintenance of the equatorial thermocline. To further assure the robustness of our conclusions, most experiments are carried out using both MOM2 and MICOM. The former is a *z*-coordinate ocean model, which has been used the most for the study of ocean circulation, while the latter is an isopycnal model, which is believed to be especially appropriate for the study of thermocline ventilation. The experiments are carried out in an idealized model domain of (20°S–60°N, 0°–60° long) (0, 4 km) with a 2° × 2° horizontal resolution.

We will first discuss the MOM2 simulations and leave the MICOM experiments to section 5. The MOM2 has 30 vertical levels, with the first 20 levels equally spaced in the upper 1000 m. The Gent–Mcwillaims (Gent et al. 1995) scheme is used with a background isopycnal mixing coefficient of 10^3 m^2 s^{-2}. The vertical tracer diffusivity coefficient is 10^{-5} m^2 s^{-2} for most experiments, based on the observational estimates in the thermocline (Jenkins 1991; Polzin et al. 1997; Schmitt 1999). The ocean is first spun up by the climatological annual cycle of the zonal mean North Pacific zonal wind stress (Hellerman and Rosenstein 1983) (Fig. 1a), sea surface temperature (Levitus and Boyer 1994) (Fig. 1b) and salinity (Levitus et al. 1994) (Fig. 1c). Surface temperature and salinity are restored with restoring times of 90 and 50 days, respectively.[1] Fifty years after the spinup, the upper ocean reaches a quasi-steady state. Figures 2a–d depict the annual mean surface density, barotropic streamfunction, and flows in the upper and lower thermocline. The barotropic flow is characterized by an anticyclonic subtropical gyre between 18° and

[1] More properly, the restoring time should be longer for (SSS) than for SST. Nevertheless, a subset of our experiments with different restoring times show no qualitative differences from the present experiments.

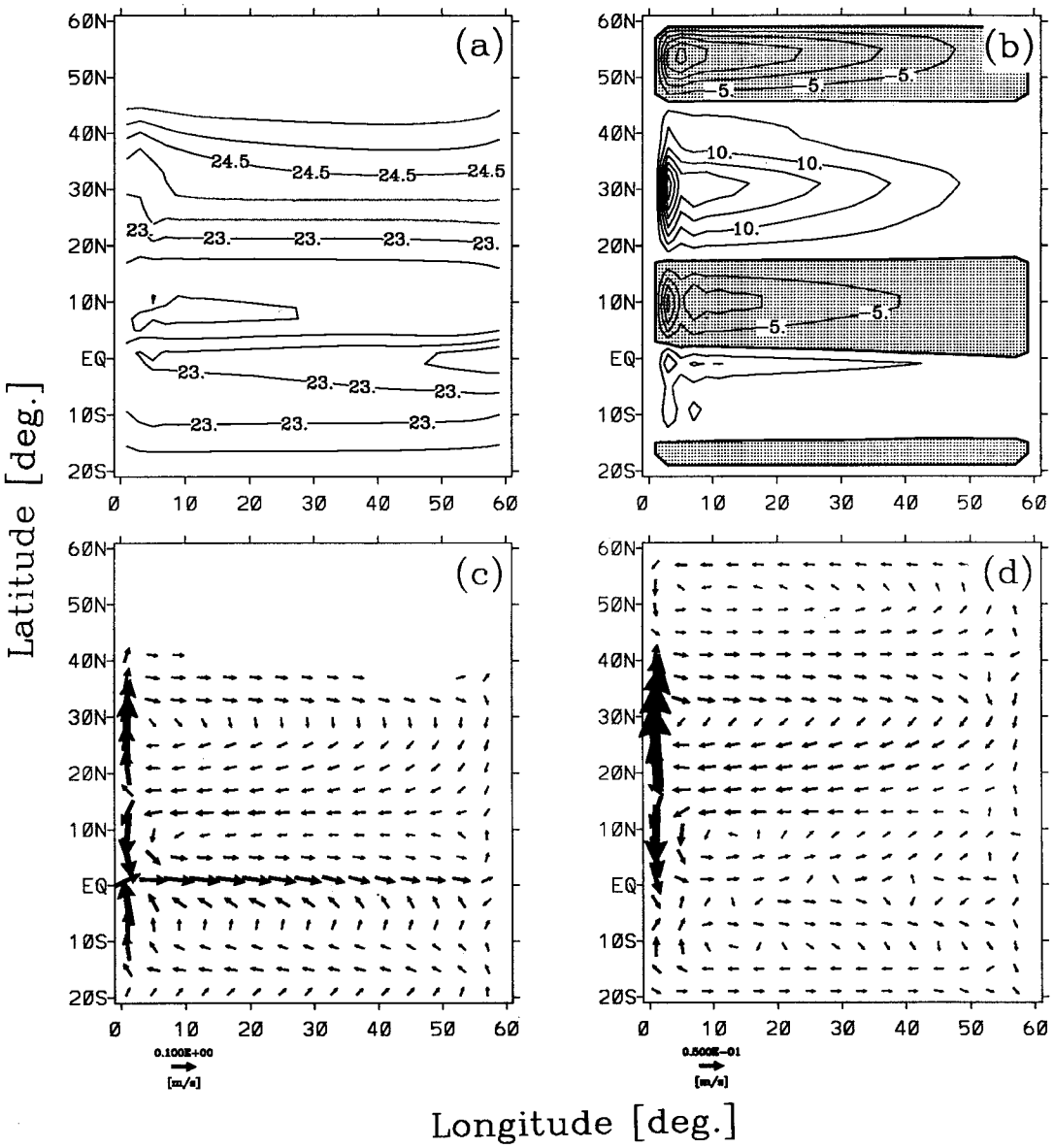

FIG. 2. Annual mean MOM2 climatology: (a) surface density (CI = $0.5\sigma_t$), (b) barotropic streamfunction (CI = 5 Sv), (c) mean upper thermocline currents (from 50 m to $25.5\sigma_\theta$), (d) lower thermocline currents (from 25.5 to $26.75\sigma_\theta$).

45°N, sandwiched by cyclonic subpolar and tropical gyres (Fig. 2b). The flows in the upper and lower thermocline show the southward subduction into the equator mainly through the low-latitude western boundary current (LLWBC).

Sensitivity experiments are performed by imposing a localized restoring SST anomaly. Table 1 lists the major MOM2 experiments to be discussed. Most experiments are forced by a sudden onset of a −2°C restoring SST cooling anomaly. In each experiment, the anomalous restoring SST is spatially uniform within the forcing region specified in Table 1. Two major groups of experiments (see Table 1) will be discussed here to test the latitude (Y1–Y4) and period (T1–T4) of the buoyancy forcing. To better understand the subduction process, a passive tracer is also applied with the source simulated by a restoring surface tracer anomaly identical to the anomalous restoring SST. The tracer can be thought either as the idealization of the observed thermocline passive tracer such as tritium and CFC (Fine et al. 1987; Jenkins 1991) or as the salinity-compensated temperature anomaly, which may also be important for subduction variability (Miller et al. 1998)

3. Optimal latitudes for buoyancy forcing

At timescales longer than decadal, the midlatitude region appears to be the optimal region for surface buoyancy

TABLE 1. MOM2 experiments. All experiments have the vertical diffusivity of 0.1×10^{-4} m^2 s^{-2}.

Expt	Forcing			Integration time (yr)	Comments
	Latitude	Longitude	Amplitude (°C)		
Y1	10°–20°N	0°–60°	−2	100	
Y2	20°–30°N	0°–60°	−2	100	
Y3	30°–40°N	0°–60°	−2	100	
Y4	40°–50°N	0°–60°	−2	100	
Y1tr	10°–20°N	0°–60°	0	30	
Y2tr	20°–30°N	0°–60°	0	30	
Y3tr	30°–40°N	0°–60°	0	30	
Y4tr	40°–50°N	0°–60°	0	30	
Yb1	10°–20°N	0°–60°	+2	30	
Yb2	20°–30°N	0°–60°	+2	30	
Yb3	30°–40°N	0°–60°	+2	30	
Yb4	40°–50°N	0°–60°	+2	30	
T1	30°–40°N	20°–40°	2	100	5-yr period
T2	30°–40°N	20°–40°	2	100	10-yr period
T3	30°–40°N	20°–40°	2	100	30-yr period
T4	30°–40°N	20°–40°	2	100	100-yr period
X2	30°–40°N	20°–40°	−2	100	

forcing to affect the equatorial thermocline. This may counter the intuition that forcing closer to the equator should produce a larger equatorial response. We present in Fig. 3 four experiments, Y1, Y2, Y3, and Y4, which are forced in the latitude bands of 10°–20°N, 20°–30°N, 30°–40°N, and 40°–50°N, respectively, and which will be referred to crudely as the cases of tropical, subtropical, midlatitude and subpolar forcing, respectively. The anomalous temperatures are averaged above $26.75\sigma_\theta$ (roughly the bottom of thermocline). The cooling on the equatorial thermocline (5°S–5°N average) intensifies with time in all cases (Fig. 3a) with most of the cooling occurring in the first 30 years. In the first three years, the equatorial response is the strongest for the tropical forcing (Y1), second for the subtropical forcing (Y2), third for the midlatitude forcing (Y3), and weakest for the subpolar forcing (Y4). The weak response for forcing away from the equator implies that, at interannual timescales, the equatorial thermocline tends to be influenced locally by buoyancy forcing close to the equator. On decadal or longer timescales, however, the equatorial response is dominated by remote forcing, initially from the subtropics, but eventually from the midlatitudes. Therefore, at decadal or longer timescales, remote forcing, especially the midlatitude forcing, is the most effective in affecting the equatorial thermocline. This response to remote midlatitude forcing should be associated with the equatorward ventilation process (Liu et al. 1994; McCreary and Lu 1994), as indicated by the temperature anomaly in the latitude–depth plot of Fig. 4c. Surface cold water subducts along isopyancal surfaces to reach the equator (Fig. 4c), mainly in the western part of the tropical ocean (including LLWBC), resulting in a significant equatorial cooling that diminishes eastward in the thermocline (Fig. 4d). The reason why midlatitude forcing is the most effective will be discussed later.

The response in the equatorial ocean is concentrated in the main thermocline, as shown in Fig. 4d. Figures 5a (Y1), 5c (Y2), 5e (Y3), and 5g (Y4) plot the vertical profiles of the zonal mean equatorial temperature anomaly (5°S–5°N average) at years 5 (dot), 15 (dash), and 30 (thin solid). It is seen that, first, all temperature anomalies reach maxima in the main thermocline. Second, consistent with Fig. 3a, the equilibrium is achieved later as the forcing region moves away from the equator (Y1 to Y4). Finally, the maximum temperature anomaly descends from about 100 m in Y1 to deeper than 200 m in Y4 because subduction occurs on denser isopycnals with forcing at higher latitudes.

The temperature response of the equatorial thermocline can be better understood when compared to a passive tracer response. Figure 3b is the same as Fig. 3a but for tracers. At first glance, the evolution of tracers closely resembles the corresponding temperature anomalies. For example, in the initial 3 years, the equatorial tracer response is the strongest in Y1, second in Y2, third in Y3, and weakest in Y4; after 15 years, the midlatitude and subtropical forcing produce the strongest and the second strongest responses, respectively.[2] The structure of the subducted tracer (Figs. 4e,f) also compares well with that of the temperature anomaly (Figs. 4c,d). Since a passive tracer is determined by advection (and eddy mixing), the similarity of the tracer and temperature anomaly patterns implies that ventilation advection plays an important role in determining the temperature response in the equatorial thermocline. In the extratropical thermocline, the ventilation of a temperature anomaly can be understood as the propagation of higher baroclinic planetary wave modes that are advected mainly by the mean thermocline flow (Liu 1999). This results in some resemblance of subduction process between an active tracer (such as temperature) and a passive tracer (Liu and Shin 1999).

Why is the midlatitude the optimal forcing region to generate a response in the equatorial thermocline? To answer this question, we should realize that the equatorial response is the result of two processes: the local response associated with the mixed layer convection and subduction and the remote response associated with the equatorward ventilation. Either a stronger local response or a higher capability of equatorward penetration favors a greater equatorial response. We first examine the local temperature response as plotted in Fig. 3c, which depicts the evolution of a local temperature anomaly in the upper ocean. In contrast to the equatorial response (Fig. 3a), the local response increases from Y1 to Y2, to Y3, and finally to Y4, indicating a poleward enhancement of the local response. This poleward enhancement is

[2] The equatorial response tends to be affected more by forcing at higher latitudes with either the increase of the thickness of the temperature (tracer) to be averaged or the time of integration. But our conclusion remains qualitatively unchanged.

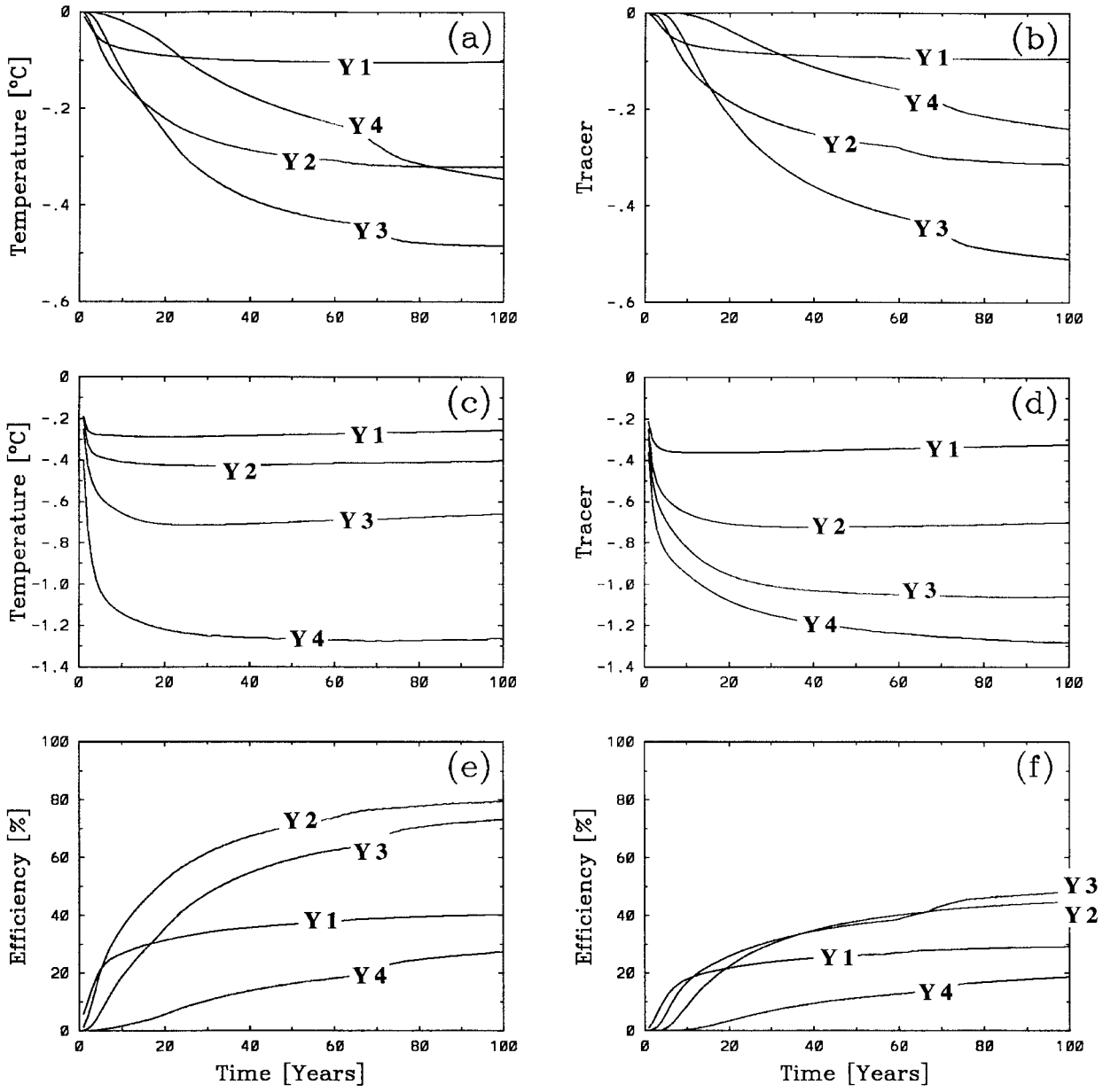

FIG. 3. Evolution of annual mean temperature anomalies and passive tracers for runs Y1, Y2, Y3, and Y4 averaged above $26.75\sigma_\theta$: (a) equatorial (5°S–5°N average) temperature anomalies, (b) equatorial tracers, (c) local temperature anomalies (averaged in the area of the anomalous forcing, e.g., between 10° and 20°N for Y1, between 20° and 30°N for Y2, etc.), and (d) local tracers. The EEP is calculated for (e) temperature anomalies and (f) tracers. The EEP for each experiment is simply calculated as the ratio of the equatorial response in (a) [or (b)] divided by the local response in (c) [or (d)].

mainly caused by a poleward deepening of the mixed layer and the thermodynamic air–sea negative feedback [which is simulated here by the surface restoring (Haney 1973)]. A deeper mixed layer allows the surface anomaly to penetrate deeper into the ocean where the temperature anomaly can be insulated effectively from the negative surface air–sea feedback. (Similar characteristics also apply to the local response of tracers in Fig. 3d.) Since the local response increases poleward, we should expect the equatorial response to increase when the forcing moves from the Tropics toward the midlatitude (Fig. 3a).

The local response argument, however, cannot explain the weak equatorial response due to subpolar forcing (Fig. 3a), which has the greatest local response (Fig. 3c), but only a modest equatorial response. The ineffectiveness of the subpolar forcing on the equator has to be associated with a poor *efficiency of equatorward*

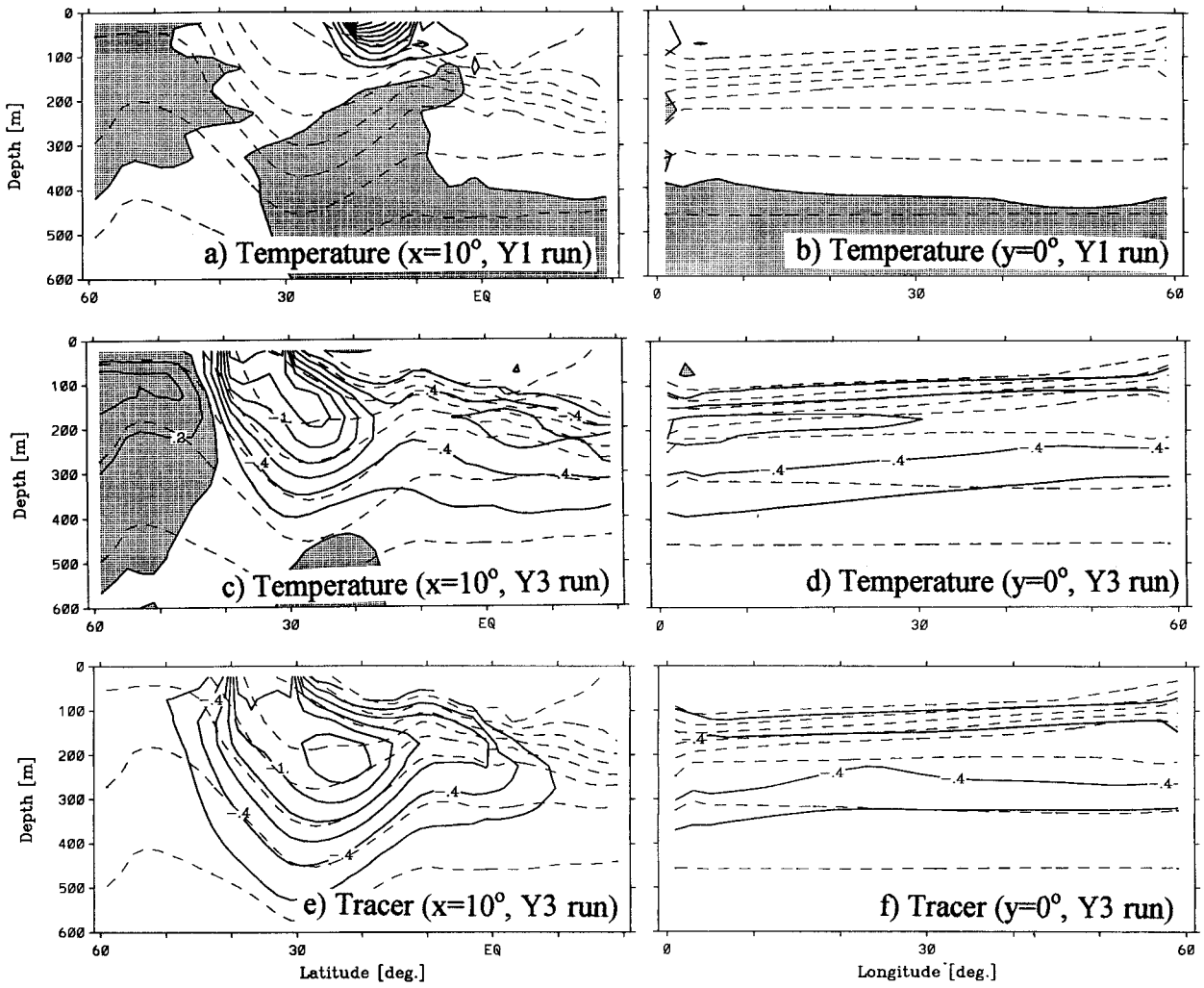

FIG. 4. Western basin meridional (5°–15° average) and equatorial zonal (5°S–5°N average) sections of temperature anomalies (positive shaded, CI = 0.2°C) and tracers (CI = 0.2) at year 30. (a) The meridional and (b) zonal sections of temperature anomalies for the tropical forcing run Y1; (c) and (d) are the same as (a) and (b) respectively but for the midlatitude forcing run Y3; (e) and (f) are respectively, the meridional and zonal sections of tracer in Y3. Dash lines are the mean isopycnals.

penetration (EEP). Two factors can contribute to a poor EEP for the subpolar forcing. First, the temperature anomaly penetrates deeper in the subpolar region where the thermocline flow is weaker (Fig. 2d) relative to the upper thermocline flow (Fig. 2c), and therefore less efficiently advects the temperature anomaly equatorward. Second, the initial anomaly is first advected poleward in the subpolar gyre (Fig. 2d), which is then recirculated and mixed strongly within the subpolar gyre before entering the subtropical gyre.

To better quantify EEP, we define

$$\text{EEP} = \langle T \rangle_{\text{EQ}} / \langle T \rangle_{L}, \tag{1}$$

where T is the temperature anomaly (or tracer) and $\langle\ \rangle_{\text{EQ}}$ and $\langle\ \rangle_{L}$ stand for the volume average (across the zonal width of the basin and above the bottom of the thermocline) in the equatorial and local forcing latitude regions, respectively. Figure 3e plots the evolution of the temperature EEPs for Y1–Y4. All the EEPs increase with time, reflecting the delay of the equatorward pen-

→

FIG. 5. Vertical profiles of equatorial temperature anomalies and tracers averaged within (0, 60°) × (5°S, 5°N) at years 5 (dotted), 10 (dash), and 30 (solid): (a), (c), (e), and (g) temperature anomalies for runs Y1, Y2, Y3, and Y4 respectively; the annual mean temperature of the control run also plotted with a heavy solid line in each panel, and (b), (d), (f), and (h) tracers of runs Y1, Y2, Y3, and Y4 respectively.

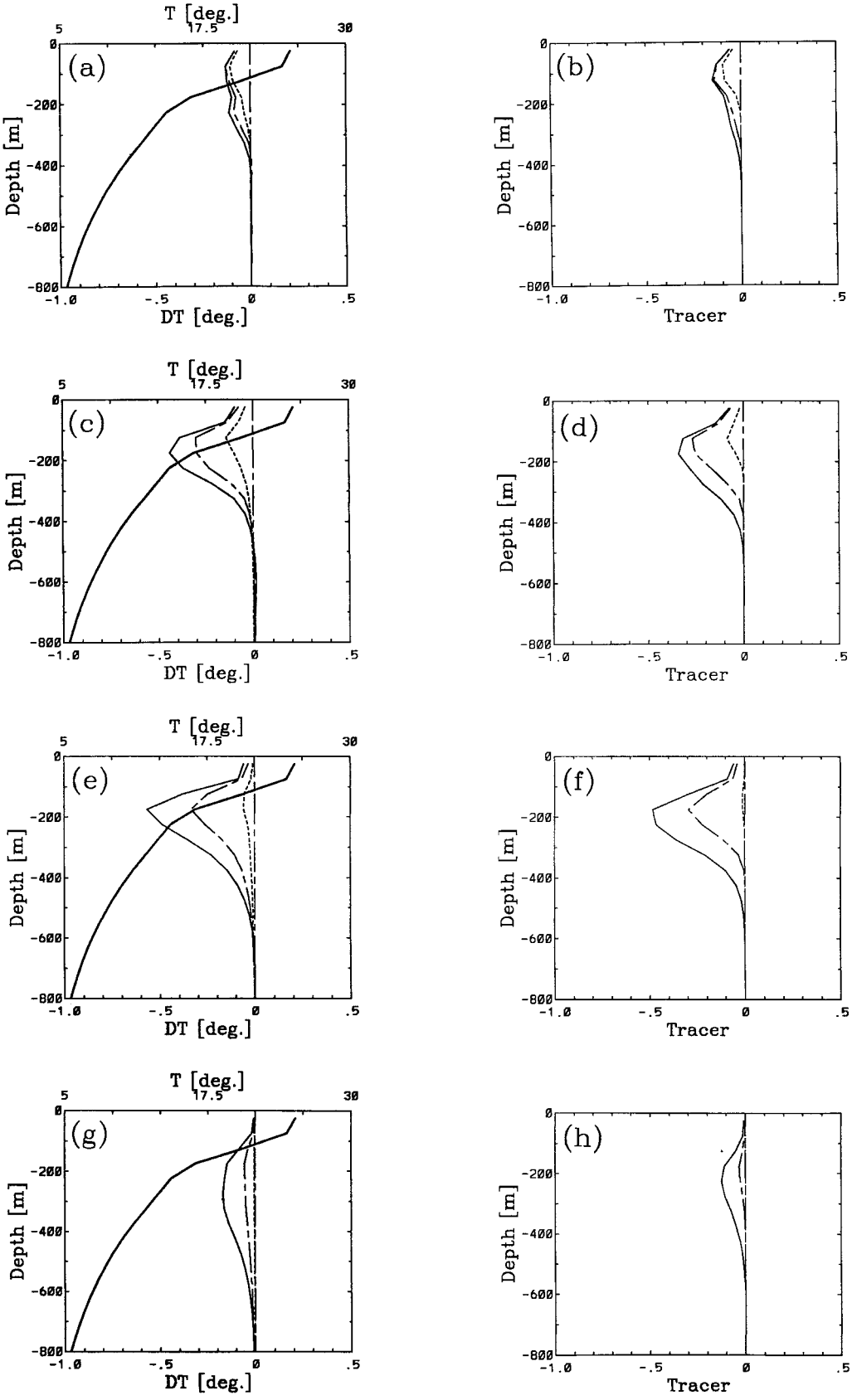
T [deg.]
5
17.5
30
(a)
(b)
(c)
(d)
(e)
(f)
(g)
(h)
Depth [m]
0
-200
-400
-600
-800
-1.0
-.5
0
.5
DT [deg.]
Tracer

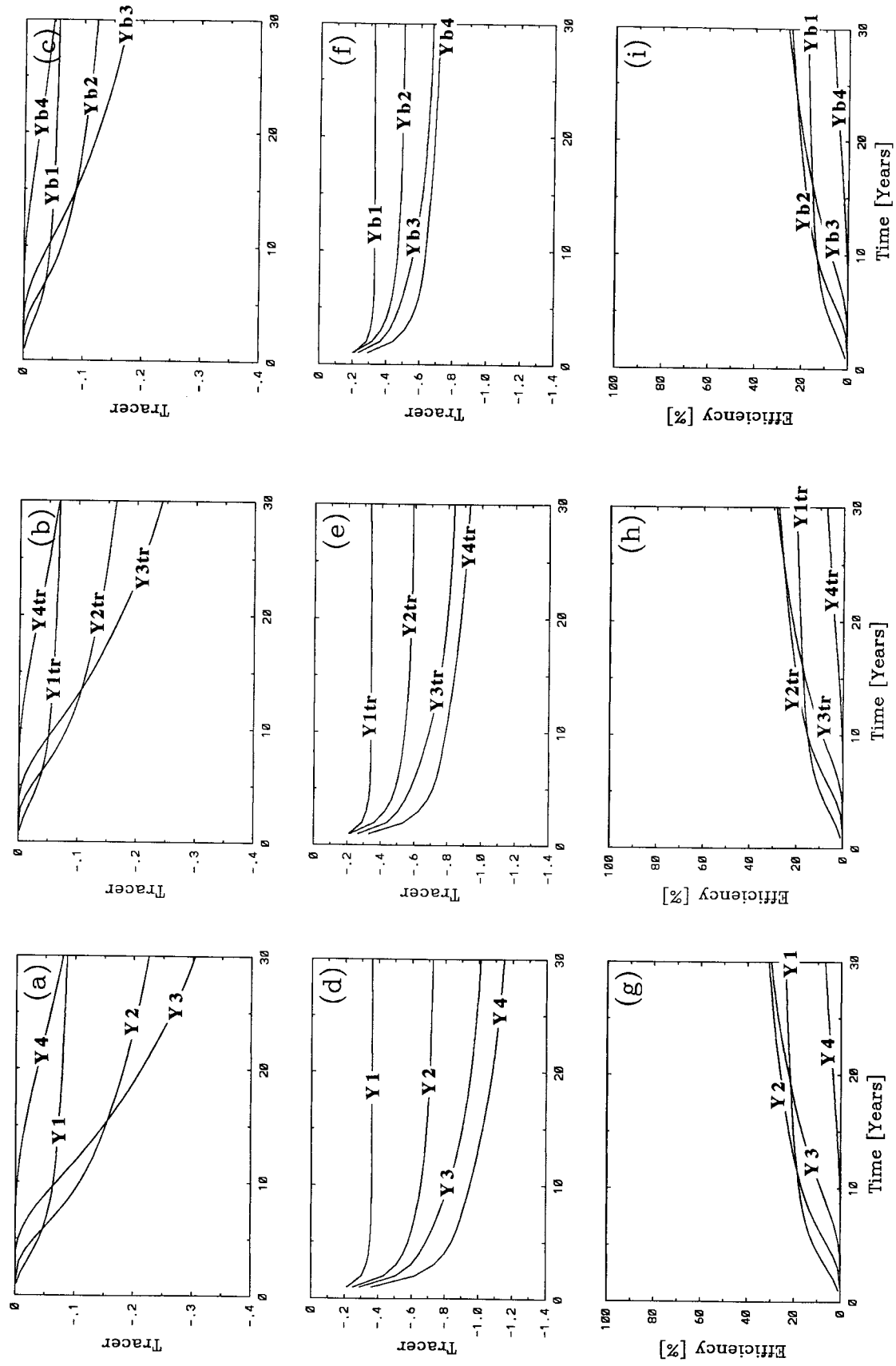

FIG. 6. Evolution of the annual mean tracer (above $26.75\sigma_\theta$) for three sets of runs, Left panels show runs Y1, Y2, Y3, and Y4 in which a −2°C anomalous cooling forcing was imposed; middle panels show runs Y1tr, Y2tr, Y3tr, and Y4tr in which no anomalous buoyancy forcing was imposed; right panels show runs Yb1, Yb2, Yb3, and Yb4 in which a +2°C anomalous warming forcing was imposed. (a)–(c) The equatorial tracer anomalies (averaged between 5°S and 5°N); (d)–(f) the local tracer anomalies; and (g)–(i) the EEPs.

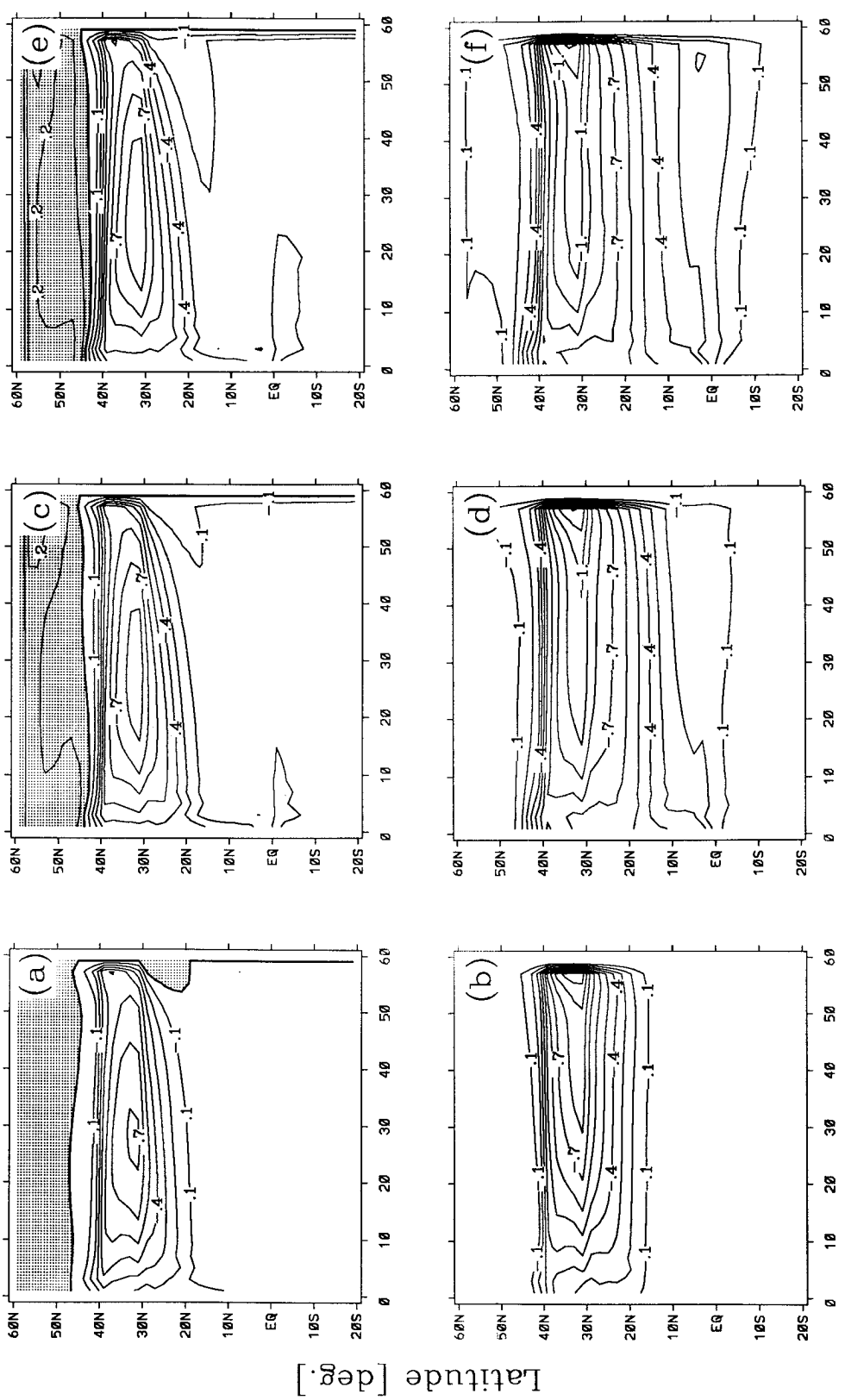

FIG. 7. The upper ocean (above 26.75σ_θ) mean temperature anomaly and a tracer for run Y3. Year 5 (a) temperature anomaly and (b) tracer, year 15 (c) temperature anomaly and (d) tracer, and year 25 (e) temperature anomaly and (f) tracer. (CI = 0.1°C for the temperature and 0.1 for the tracer.)

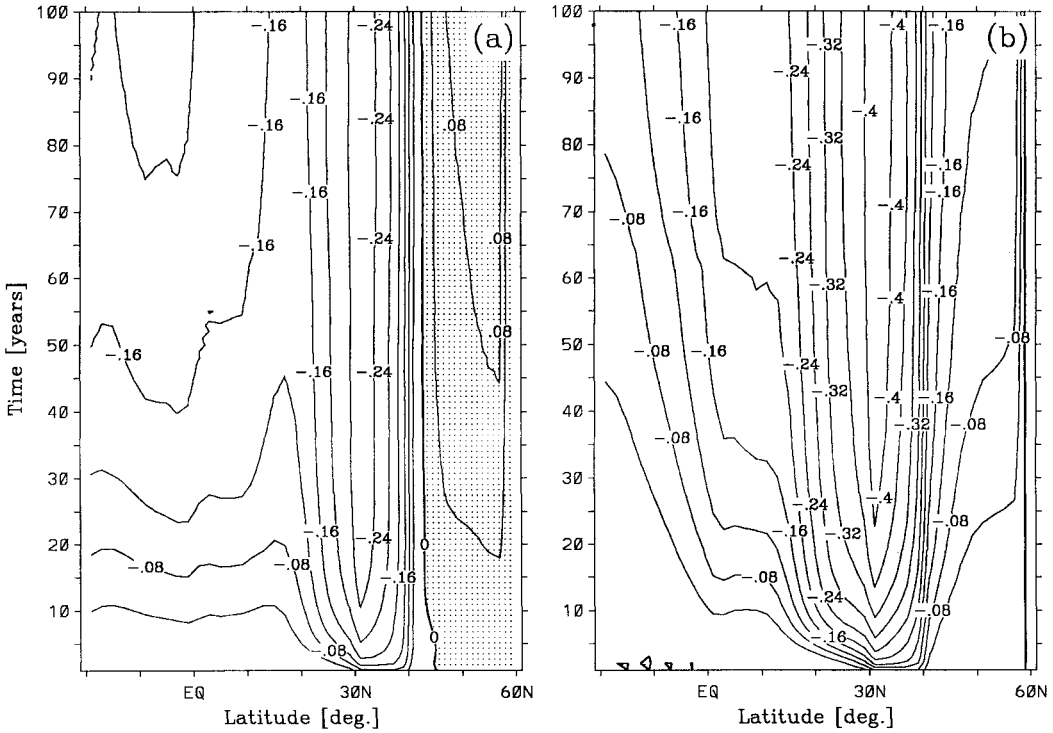

FIG. 8. Latitude–time plot of the zonal mean (a) temperature anomaly and (b) tracer for run X2.

etration process. After about 10 yr, the greatest EEPs are achieved by the subtropical and midlatitude forcing (70% at year 100). In contrast, the tropical and subpolar forcing have rather low EEP. The midlatitude region is therefore unique in that it generates a strong local response and has a high EEP (at least on interdecadal timescales). Consequently, forcing in the midlatitudes most efficiently affects the equatorial thermocline.

It is important to recognize that, in spite of some similarities, temperature anomalies and tracers do have significant differences. This point has been discussed for the midlatitudes (Liu and Shin 1999). The difference will become even more striking in the MICOM experiments as will be discussed later. The responses have different spatial structures as shown in our experiments here. While the tracer retains the same sign as the forcing over the entire ocean (Fig. 4e), the temperature anomaly exhibits a broad, albeit weak, warming beneath a strong cooling in the upper thermocline (between 18° and 40°N; Fig. 4c), resembling the structure of a second baroclinic mode (Liu 1999). This second modelike response is even more clear for the case of the tropical forcing (Y1 run in Fig. 4a). These baroclinic responses can also be seen in the steady ventilated thermocline model, as shown by Huang and Pedlosky (1999), Schneider et al. (1999), and more generally in our appendix. Furthermore, in the equatorial region, the temperature anomaly signal is stronger than that of the tracer: the temperature anomaly has a submaximum around the equator (Fig. 4c), while the tracer diminishes monotonically southward (Fig. 4e).

Most strikingly, the temperature EEP (Fig. 3e) is significantly higher than the tracer EEP (Fig. 3f). This is especially true in the cases of subtropical (Y2) and midlatitude (Y3) forcing, where the temperature EEP is almost twice the tracer EEP. This *high temperature EEP* is the most *robust and interesting* result of this paper. One direct implication is that a naive tracer analogy for temperature anomaly subduction will underestimate the equatorward propagation of the temperature anomaly substantially. Before further exploring the dynamic implications of the high temperature EEP, we first explain a subtle feature of the tracer response.

A low tracer EEP should favor a weak tracer response at the equator relative to temperature. Yet, in runs Y1–Y4, tracers have equatorial responses (Fig. 3b) comparable to that of temperature anomalies (Fig. 3a). The reason is that the tracer has a substantially stronger local response (Fig. 3d) than the temperature (Fig. 3d), especially in Y2 and Y3. The strong local tracer response is, however, mainly caused by the accompanying surface cooling forcing in runs Y1–Y4. The cooling anomaly enhances mixed layer convection, which favors a stronger downward tracer penetration. To demonstrate this, two additional sets of experiments (Y1tr–Y4tr and Yb1–Yb4, see Table 1) are performed, in which the surface tracer is applied the same as in Y1–Y4. The anomalous temperature forcing, however, is not applied in Y1tr–Y4tr, and is applied as a +2°C warming in Yb1–Yb4. Figure 6 plots the 30-yr evolution of equatorial and local responses as well as EEPs for the three sets of experiments. One dramatic feature is that the

EEP is affected little by the anomalous temperature forcing. This is reasonable because the tracer EEP is determined purely by the mean thermocline ventilation, which is changed little by the perturbation temperature in the forcing region. In contrast, the local tracer response weakens significantly, from the runs with cooling forcing (Y1–Y4, Fig. 6d), to the runs without cooling (Y1tr–Y4tr, Fig. 6e), and further to the runs with warming forcing (Yb1–Yb4, Fig. 6f). As a result, the equatorial response is reduced by about 20% with a 2°C warm anomaly (cf. Figs. 6a,d,g with Figs. 6b,e,h or cf. Figs. 6b,e,h with Figs. 6c,f,i).

The high temperature EEP (relative to tracer) implies that wave dynamics contribute significantly to the temperature response in the equatorial thermocline. Since the EEP of temperature could reach twice that of tracer (for Y2 and Y3), the contribution of wave dynamics to the equatorial response is comparable to advection. There are at least two mechanisms that are responsible for the large temperature EEP. First, coastal Kelvin waves can carry temperature anomalies toward the equator at the western boundary, which has been suggested to contribute to decadal equatorial climate variability (Lysne et al. 1997; Liu et al. 1999). Although distorted by the coarse model resolution, the coastal Kelvin wave should still operate in our model (Hsieh et al. 1983) and therefore enhance the temperature EEP. Second, baroclinic waves have a strong westward propagation component in addition to mean flow advection. This is particularly true for the first mode of the baroclinic planetary wave, whose propagation is controled strongly by the non-Doppler-shift effect (Killworth et al. 1997; Dewar 1998; Liu 1999). A temperature signal can therefore rapidly propagate to the western boundary as a baroclinic Rossby wave, which is then brought to the equator by either a coastal Kelvin wave or the LLWBC.

The two mechanisms discussed above are supported by further analyses. Figure 7 presents snapshots of upper-ocean temperature anomalies (Figs. 7a,c,e) and tracers (Figs. 7b,d,f) at years 5, 15, and 25. The temperature anomaly shows a clear penetration tongue along the western boundary into the equator (Figs. 7a,c,e), which is virtually absent in the tracer (Figs. 7b,d,f). This temperature tongue forms because both the coastal Kelvin wave and the LLWBC travel much faster than the interior equatorward ventilation flow. It is this temperature tongue that results in the equatorial submaximum temperature anomaly discussed in Fig. 4c. Figure 8 plots the time–latitude plot of the temperature anomaly (Fig. 8a) and tracer (Fig. 8b) averaged zonally across the basin and vertically in the upper ocean. The cooling anomaly (Fig. 8a) propagates rapidly into the equator, forming a submaximum on the equator; it then expands toward the Southern Hemisphere due to the poleward propagation of coastal Kelvin waves along the eastern boundary (not shown). In contrast, the tracer expands southward slowly (Fig. 8b) due to the subduction flow and the LLWBC; it also lacks clear penetration across the equator due to the absence of cross-equator flow in the thermocline. The weak tracer penetration across the equator is due to horizontal mixing.

In short, the midlatitude appears to be the optimal region for buoyancy forcing to affect the equatorial thermocline. Both advection and wave propagation are important for the temperature response in the equatorial thermocline.

4. Response to forcing at different timescales

We now investigate the response of the equatorial thermocline to midlatitude forcing at various time scales. Earlier discussions (Fig. 3) indicate that the equatorial response intensifies with time, becoming significant only on interdecadal timescales. For a periodic buoyancy forcing, we therefore speculate that the equatorial response increases with the forcing period, and that the equatorial response will become significant only when the forcing period reaches interdecadal. These speculations seem to be supported by four runs with periodic midlatitude forcing: T1 for 5-yr period, T2 for 10-yr period, T3 for 30-yr period, and T4 for 100-yr period, as well as an accompany steady forcing run X2 (see Table 1). Figures 9a–d are the same as Figs. 3a–d but for T1–T4 and X2 runs.[3]

Figure 9a shows that the temperature response in the equatorial thermocline diminishes rapidly for a high-frequency forcing (from run X2 to run T1). The amplitude for the equatorial response (A_{EQ} can be estimated as

$$
\begin{aligned}
A_{EQ}(\mathrm{X2}) &\approx [0.14 - (-0.2)]/2 = 0.17,\\
&\quad \text{steady}^4\\
A_{EQ}(\mathrm{T4}) &\approx [0.1 - (-0.15)]/2 = 0.125,\\
&\quad \text{100-yr period}\\
A_{EQ}(\mathrm{T3}) &\approx [0.02 - (-0.06)]/2 = 0.04,\\
&\quad \text{30-yr period}\\
A_{EQ}(\mathrm{T2}) &\approx [-0.02 - (-0.04)]/2 = 0.01,\\
&\quad \text{10-yr period}\\
A_{EQ}(\mathrm{T1}) &\approx [-0.06 - (-0.07)]/2 = 0.005,\\
&\quad \text{5-yr period.}
\end{aligned}
\tag{2}
$$

Steady forcing has the maximum equatorial response; the 100-yr forcing generates a response comparable with the maximum amplitude; 30-yr forcing produces a re-

[3] Note that in the equatorial response (Fig. 10a) there is a long-term mean cooling for all the periodic forcing cases even though the restoring SST forcing has no long-term mean. This cooling occurs because of a somewhat larger local response to a cooling than to a warming forcing (Fig. 10c, as discussed regarding Fig. 6 and later in the appendix). The former produces an anomalously deep mixed layer and therefore allows the thermocline temperature anomaly to be shielded from surface air–sea negative feedback.

[4] The warm peak of X2 is estimated based on the ratio of the warm and cold peaks of run T4. This is also true in other estimates.

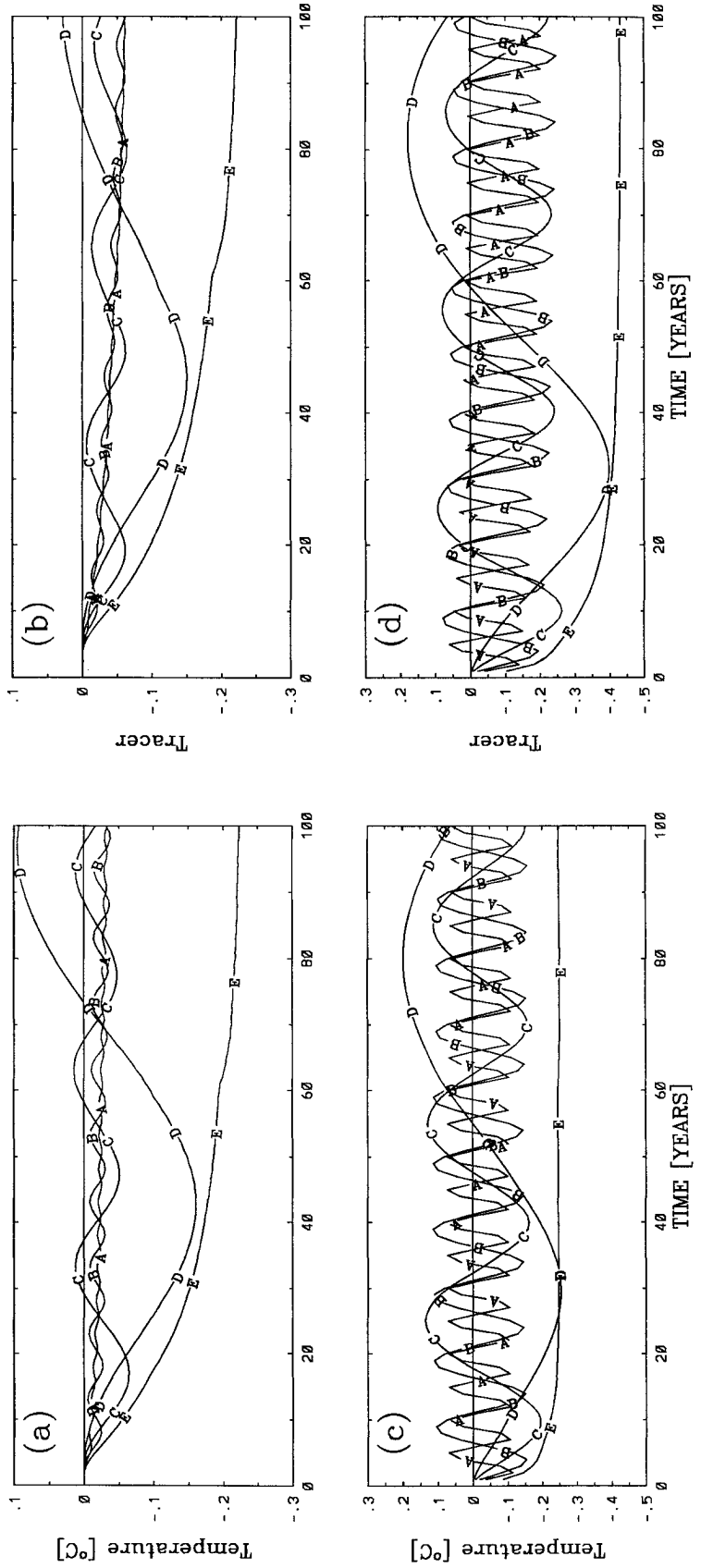

FIG. 9. Responses to periodic forcing (T1, T2, T3, T4) and steady forcing X2. Equatorial responses (above 26.75σ_θ, 5°S–5°N, 0°–60°) of (a) temperature anomalies and (b) tracers, local responses (above 26.75σ_θ, 30°–40°N, 0°–60°) of (c) temperature anomalies and (d) tracers.

sponse about one quarter of the maximum response. Decadal and interannual forcing, however, produce much weaker responses. Therefore, in our model ocean, only a forcing of interdecadal period can generate a significant response on the equatorial thermocline.

The weak equatorial response at high frequencies is associated primarily with their poor EEPs, rather than their local responses. Figure 9c shows that the local temperature response decreases for a higher-frequency forcing, with the amplitude (A_L) of

$$\begin{aligned} A_L(\text{X2}) &\approx [0.21 - (-0.25)]/2 = 0.23, && \text{steady}\\ A_L(\text{T4}) &\approx [0.2 - (-0.25)]/2 = 0.225, && \text{100-yr period}\\ A_L(\text{T3}) &\approx [0.15 - (-0.2)]/2 = 0.175, && \text{50-yr period}\\ A_L(\text{T2}) &\approx [0.1 - (-0.15)]/2 = 0.125, && \text{10-yr period}\\ A_L(\text{T1}) &\approx [0.07 - (-1.1)]/2 = 0.09, && \text{5-yr period.} \end{aligned} \tag{3}$$

As the forcing frequency increases, the local response decreases, but much slower than the equatorial response. A careful comparison shows that the reduction of the equatorial response in (2) dramatically exceeds that of the local response in (3). For example, the equatorial response is reduced by one order from the steady (X2) to the interannual forcing (T1), while the local response is reduced only by one half. The implication is a dramatic reduction of the EEP for a higher frequency. In the case of periodic forcing, the definition of EEP can be modified from (1) as the ratio of the amplitudes of the equatorial and local responses:

$$\text{EEP} = A_{\text{EQ}}/A_L.$$

Using both (2) and (3), we have

$$\begin{aligned} \text{EEP(X2)} &\approx 73\%, && \text{steady}\\ \text{EEP(T4)} &\approx 55\%, && \text{100-yr period}\\ \text{EEP(T3)} &\approx 23\%, && \text{50-yr period}\\ \text{EEP(T2)} &\approx 8\%, && \text{10-yr period}\\ \text{EEP(T1)} &\approx 5\%, && \text{5-yr period.} \end{aligned} \tag{4}$$

The EEP decreases rapidly for high frequency forcing. Therefore, the weaker equatorward ventilation process is the primary cause for the weak equatorial response at high frequencies.

The tracer response (Figs. 9b,d) also shows many similarities to the temperature anomaly (Figs. 9a,c). This similarity again implies that advection plays an important role in the equatorial response. For example, the tracer shows a dramatic reduction in the equatorial response towards the high frequency (Fig. 9b; more than 10 times from runs X2 to T1), although the local response (Fig. 9d) shows only a modest reduction (about 4 times from runs X2 to T1).[5] The mechanism for the much reduced EEP at high frequency is not entirely clear. Perhaps, a higher frequency forcing produces a disturbance of a smaller spatial scale, which is more likely to be dissipated.

The tracer EEP can be estimated from Fig. 9b and Fig. 9d as

$$\begin{aligned} \text{EEP(X2)} &\approx [0.11 - (-0.03)]/[0.2 - (-0, 1)] = 46\%, && \text{steady}\\ \text{EEP(T4)} &\approx [0.09 - (-0.02)]/[0.2 - (-0, 1)] = 36\%, && \text{100-yr period}\\ \text{EEP(T3)} &\approx [0.035 - 0.01]/[0.13 - (-0.05)] = 18\%, && \text{50-yr period}\\ \text{EEP(T2)} &\approx [0.03 - 0.022]/[0.12 - (-0.02)] = 6\%, && \text{10-yr period}\\ \text{EEP(T1)} &< 1\%, && \text{5-yr period.} \end{aligned} \tag{5}$$

The tracer EEPs are less than half the corresponding temperature EEPs in (4). This is consistent with the steady forcing cases discussed in section 3 (Figs. 3e and 3f). As discussed before, the enhancement of the temperature EEP over the tracer is caused by dynamic waves.

It is interesting to point out that the temperature anomaly penetrates equatorward stronger than the tracer only in the Tropics (south of 15° to 20°N). This can be observed in the time–latitude plot of the zonal mean temperature anomaly (Fig. 10a) and tracer (Fig. 10b) for run T3. The temperature anomaly has a clear tongue of penetration into and across the equator, forming a submaximum around the equator (Fig. 10a), while the tracer diminishes monotonically southward (Fig. 10b). In the Tropics (south of about 15°N), the temperature anomaly propagates rapidly with the amplitude virtually unchanged (Fig. 10a) while the tracer tongue progresses slowly with a severe amplitude reduction. The opposite occurs in the subtropics (north of about 15°N): the temperature anomaly propagates southward slowly with the amplitude decreased rapidly, forming a temperature front at about 20°N; the tracer, however, advances southward rather fast with only a weak attenuation of the amplitude, forming a tracer front at about 10°N. The difference between temperature anomaly and the tracer can also be seen in the steady forcing case in Fig. 8. The net cumulative effect on the equatorial temperature seems to be overwhelmed by the tropical process, resulting in a high temperature EEP. This highlights the

[5] The tracer shows a negative long term mean even with a periodic source restoring tracer forcing. This is because the tracer released during the cooling period is stronger than that released during the warming season, as shown in Fig. 6.

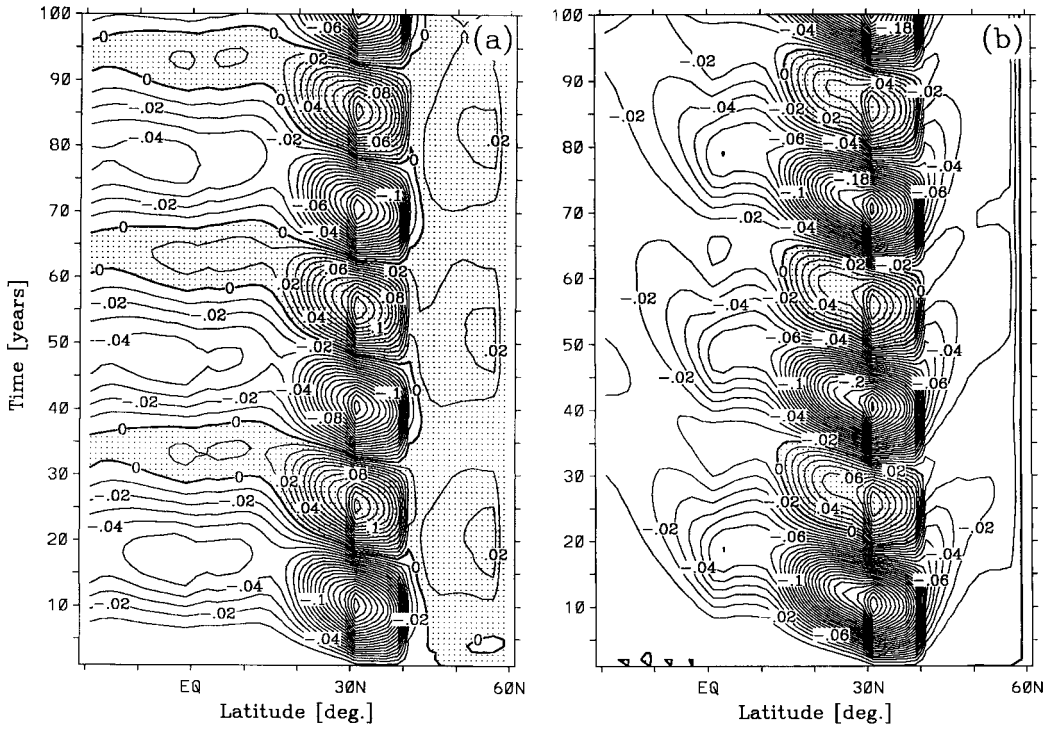

FIG. 10. Same as Fig. 8 but for run T3.

importance of the tropical process in extratropical–tropical exchanges.

Why does the temperature propagate differently in the Tropics and in the subtropics? We will offer one interpretation. In the subtropical thermocline, a subduction temperature anomaly represents a high baroclinic mode, which may propagate substantially slower than a tracer, and whose amplitude decreases faster than a passive tracer due to the divergence or group velocity field (Liu 1993; Stephens et al. 2000). This may account for the slower propagation and rapid weakening of the temperature anomaly than the tracer in the subtropics. In the Tropics, the equatorward penetration occurs predominantly in the western boundary region where the coastal Kelvin wave may significantly enhance the propagation of the temperature anomaly, but not the tracer.

TABLE 2. MICOM experiments. Except as noted, all experiments are forced by a sudden onset of steady anomalous forcing and integrated for 30 yr with a diapycnal diffusivity of $K_{\text{diapycnic}} \times N = 0.6 \times 10^{-7}$ m^2 s^{-2}, where N is the Brunt–Väisälä frequency.

	Forcing			
Expt	Latitude	Longitude	Amplitude (°C)	Comments
MY1	10°–20°N	0°–60°	−2	
MY2	20°–30°N	0°–60°	−2	
MY3	30°–40°N	0°–60°	−2	
MY4	40°–50°N	0°–60°	−2	
MT1	30°–40°N	20°–40°	2	5-yr period
MT2	30°–40°N	20°–40°	2	10-yr period
MT3	30°–40°N	20°–40°	2	30-yr period
MT4	30°–40°N	20°–40°	2	100-yr period
MX2	30°–40°N	20°–40°	−2	
MYa1	10°–20°N	0°–60°	−1	
MYa2	20°–30°N	0°–60°	−1	
MYa3	30°–40°N	0°–60°	−1	
MYa4	40°–50°N	0°–60°	−1	
MYb1	10°–20°N	0°–60°	+2	
MYb2	20°–30°N	0°–60°	+2	
MYb3	30°–40°N	0°–60°	+2	
MYb4	40°–50°N	0°–60°	+2	

5. MICOM simulations

Most conclusions from the MOM2 experiments are confirmed by MICOM. The MICOM is configured and forced the same as the MOM2, and has 11 isopycnal layers ($23\sigma_\theta$, $24\sigma_\theta$, $25\sigma_\theta$, $25.5\sigma_\theta$, $26\sigma_\theta$, $26.25\sigma_\theta$, $26.5\sigma_\theta$, $27\sigma_\theta$, $27.45\sigma_\theta$, $27.6\sigma_\theta$, $27.7\sigma_\theta$) beneath a mixed layer. Since our MICOM is about 4 times slower than our MOM2, all the MICOM experiments are integrated only for 30 years after the onset of the anomalous forcing. Table 2 lists some MICOM experiments to be discussed here.

We first examine the response to forcing at different latitudes. Figure 11 is the same as Fig. 3 but for the four corresponding MICOM simulations MY1, MY2, MY3, and MY4, which are forced by an anomalous cooling in the tropical, subtropical, midlatitude and subpolar regions, respectively (Table 2). Major features of MOM2 experiments (Fig. 3) are reproduced here. First,

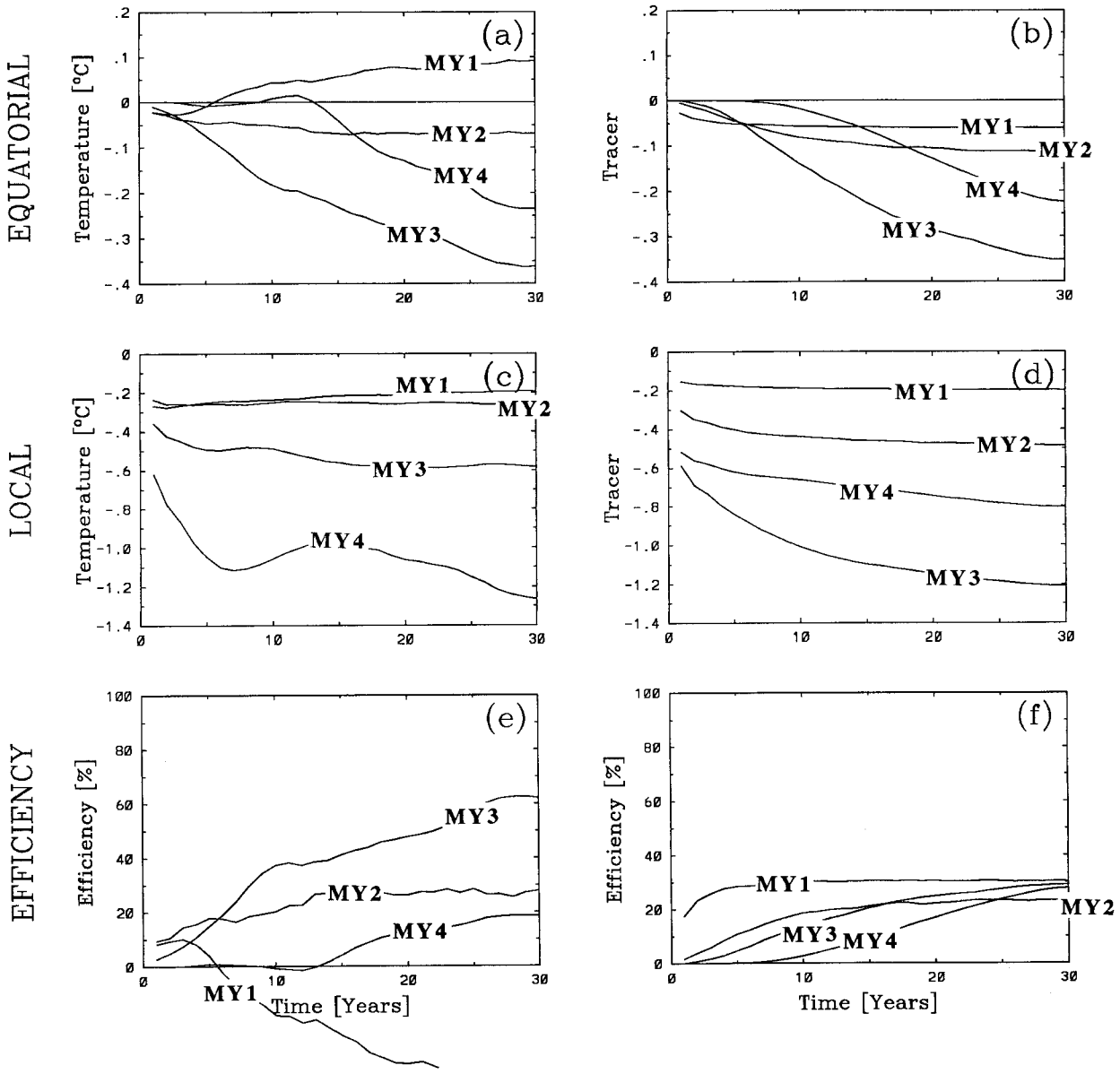

FIG. 11. Same as Fig. 3 but for MICOM experiments with forcing at different latitude bands (MY1, MY2, MY3, MY4). A 3-yr running mean is applied.

after 30 years, the midlatitude forcing generates the strongest equatorial temperature response (Fig. 11a) and has an EEP of over 50% (Fig. 11e). Second, temperature anomalies evolve similarly to tracers, confirming the role of ventilation in the equatorial response (except for the tropical forcing case MY1). Third, the temperature EEPs (Fig. 11e) are significantly higher than the tracer EEPs (Fig. 11f), confirming the important role of dynamic waves in enhancing the equatorial response of temperature anomalies. Fourth, the equatorial response becomes significant only after decadal time scales. The meridional and equatorial sections of the MY3 experiments (Figs. 12c,d) resemble the Y3 experiment (Figs. 4c,d) and the vertical profiles of equatorial response in MICOM experiments (Fig. 13) also resemble those of the MOM2 experiments (Fig. 5; except for the temperature response in MY1).

The equatorial response to midlatitude periodic forcing in MICOM (Fig. 14a) also resembles closely the MOM2 response (Fig. 9a). The equatorial response becomes significant for interdecadal forcing. In addition, to demonstrate the linear nature of the equatorial response to extratropical forcing, Figs. 14b and 14c present the equatorial temperature responses the same as

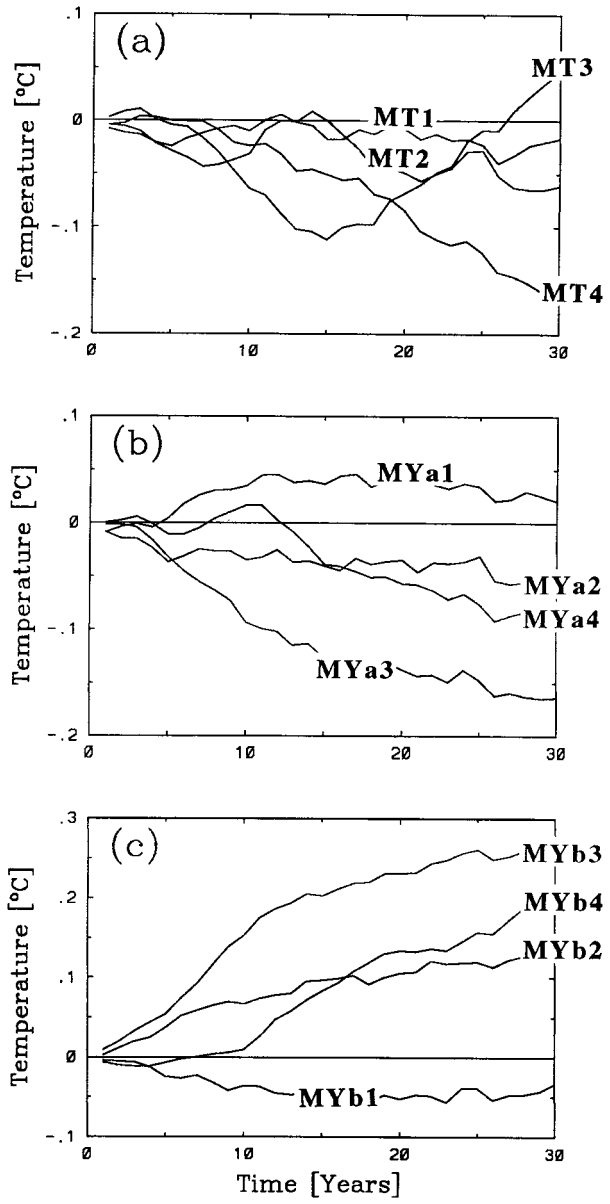

FIG. 12. Evolution of equatorial thermocline temperature anomalies ($\rho < 26.75\sigma_\theta$, 5°S $< y <$ 5°N, 0° $< x <$ 60°) for MICOM runs of (a) periodic forcing: MT1, MT2, MT3, and MT4; (b) half cooling forcing: MYa1, MYa2, MYa3, and MYa4; (c) anomalous warming forcing: MYb1, MYb2, MYb3, and MYb4 (see Table 2). A 3-yr running mean is applied.

MY1–MY4, but for half of the forcing intensity (−1°C cooling) and for the opposite sign of forcing (+2°C warming), respectively. All the major features in Figs. 14b and 14c are the same as in Fig. 11a, if the response is multiplied by 1 in Fig. 14b and by −2 in 14c (except for the tropical forcing cases MYa1 and MYb1). The amplitude is somewhat reduced for the warming forcing, which is less effective that a cooling in generating subduction as discussed regarding Fig. 6.

There are also interesting differences between MICOM and MOM2 experiments. In general, the MOM2 simulations tend to be more diffusive than the corresponding MICOM experiments, as expected. For example, the mean equatorial thermocline is much sharper in MICOM than in MOM2 (compare the mean temperature profile in Figs. 4 and 5 with those in Figs. 12 and 13). The sharper thermocline results in a sharper equatorial response in both temperature and tracer in MICOM. In addition, the temperature response under the midlatitude cooling (MY3) exhibits a clear third-modelike structure south of the forcing region (20° to 30°N) with the midthermocline cooling sandwiched by weak surface and lower thermocline warming (Fig. 12c). This response structure can be proven to be the general feature of a ventilated thermocline model as discussed in the appendix (Figs. A1c,f). In contrast, the MOM2 simulation Y3 produces little surface warming (Fig. 4c). Furthermore, the warm anomaly is advected along the LLWBC in the main thermocline all the way to the equator in MY3 (Figs. 13e,d), but is diffused before reaching the equator in Y3 (the anomaly pattern along the western boundary is virtually identical to Fig. 4c). It is clear that MOM2 is deficient in simulating subduction responses. Even though the cold anomaly penetrates across the equator in the main thermocline in both MOM2 and MICOM (Fig. 4d, Fig. 12d), only in MY3, the warm anomaly beneath the thermocline penetrates along the equator eastward slightly (Fig. 12d). In another similar experiment that is forced by the South Pacific forcing, the warm anomaly beneath the thermocline penetrates further, but still only half way across the equator (not shown). The strong penetration of cold anomaly in the main thermocline may be helped by the strong eastward Equatorial Undercurrent there. The warm anomaly beneath the thermocline, however, may be dispersed by the strong shear flow.

The MICOM and MOM2 differ most drastically in the case of tropical forcing (MY1 vs Y1). Locally under the cooling, both runs produce a second-modelike response (Fig. 12a and Fig. 4a). However, the warming anomaly is much stronger in the main thermocline in MY1 than in Y1. Furthermore, the warm anomaly in the main thermocline penetrates into the equator and generates a strong thermocline warming along the equator in MY1 (Figs. 12a,b and Fig. 13a), but it fails to generate warming in the equatorial thermocline in Y1 (Figs. 4a,b and Fig. 5a). [Instead, in Y1 run, a weak warming penetrates across the equator below the thermocline (Figs. 4a,b).] This strong midthermocline warming, in response to a tropical cooling, is consistent with the solution of the idealized ventilated thermocline model discussed in the appendix (Figs. A1a,b,d,e). There, one can show that forcing in the tropics is the most efficient in generating low-latitude midthermocline warming. This tropical forcing case provides a good example showing the difference of the active and passive tracers. This difference is most clear in MICOM.

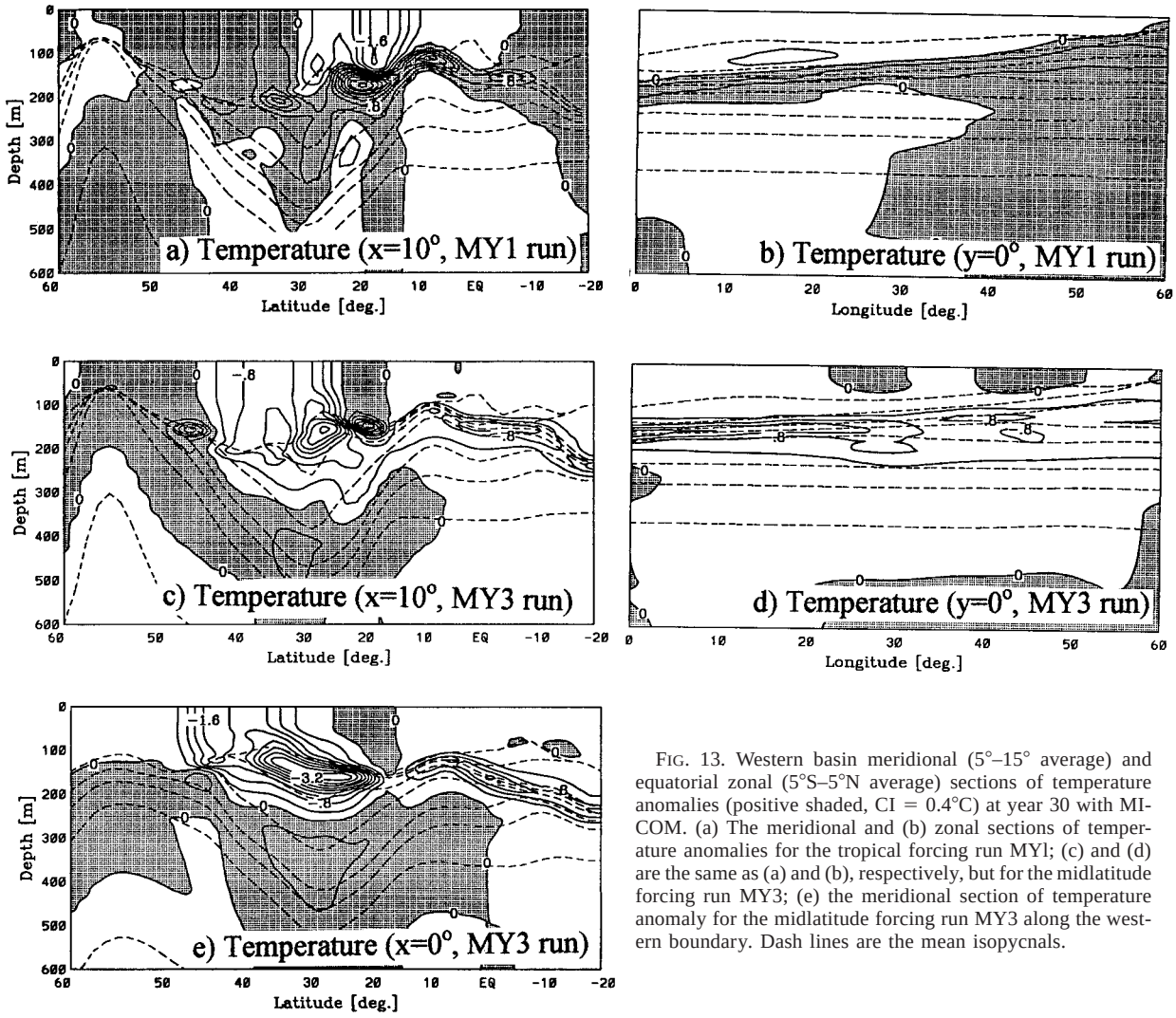

FIG. 13. Western basin meridional (5°–15° average) and equatorial zonal (5°S–5°N average) sections of temperature anomalies (positive shaded, CI = 0.4°C) at year 30 with MICOM. (a) The meridional and (b) zonal sections of temperature anomalies for the tropical forcing run MYl; (c) and (d) are the same as (a) and (b), respectively, but for the midlatitude forcing run MY3; (e) the meridional section of temperature anomaly for the midlatitude forcing run MY3 along the western boundary. Dash lines are the mean isopycnals.

6. Summary and discussion

OGCM experiments were performed systematically to investigate the response of the equatorial thermocline to extratropical surface buoyancy forcing. It is found that, first, the midlatitudes comprise the region where buoyancy forcing can generate the strongest response in the equatorial thermocline. This occurs because the midlatitudes have a strong local response and the subduction anomaly penetrates into the equator efficiently. Second, thermocline ventilation and wave dynamics are equally important in forcing temperature responses in the equatorial thermocline. Third, midlatitude forcing can exert a significant equatorial response after it persists longer than decadal timescales. A forcing shorter than decadal timescales seems to generate a midlatitude response that is rapidly damped before it reaches the equator. In addition, a tropical buoyancy forcing can generate a strong equatorial thermocline temperature anomaly that is of opposite sign as the forcing.

Extensive sensitivity experiments have also been carried out. Three experiments are performed in which the anomalous SST forcing is imposed in the western, central, and eastern third of the midlatitude region. Surprisingly, it is found that the equatorial response is comparable for the three forcing cases, especially in temperature anomalies (not shown). One might have expected a much weaker equatorial response for the forcing in the western basin because of the lack of exchange windows there (McCreary and Lu 1994; Liu et al. 1994). It appears that the western forcing case does have the smallest EEP, consistent with the notion of weak equatorward ventilation from there. However, the western forcing generates a strong local response due, perhaps, to the deeper mixed layer there.

Experiments are also carried out in MOM2 with an enhanced vertical diffusivity of 5×10^{-5} m^2 s^{-2}. This diffusivity, five times larger than that of our previous experiments, seems to be large compared to observa-

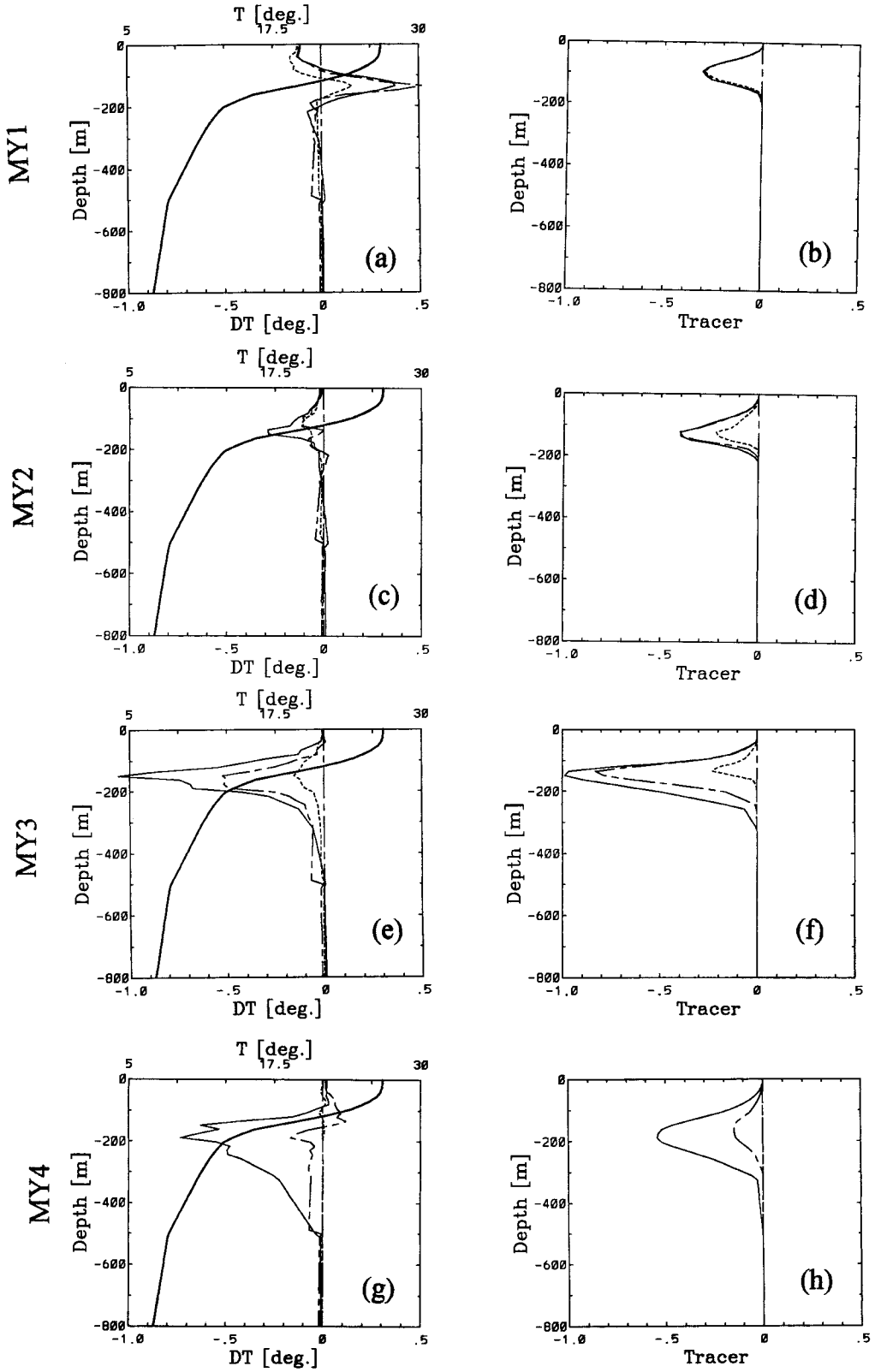

FIG. 14. Same as Fig. 5 but for MICOM runs MY1, MY2, MY3, and MY4.

tional estimates in the thermocline, but still comparable to that of the deeper ocean (Jenkins 1991; Polzin et al. 1997; Schmitt 1999). The large diffusivity only changes our conclusions quantitatively. The larger diffusivity weakens the equatorial response by about 40% to 70%, with more reduction in the local response than in the EEPs. Physically, a large diffusivity allows the local anomaly to penetrate deeper below the thermocline, leaving less of an anomaly within the thermocline. Therefore, the local thermocline response is reduced. Diffusion also weakens the advective and dynamic waves, and in turn the EEP.

In another set of experiments, salinity-compensated anomalous SST forcing is applied. The subduction temperature anomaly behaves virtually the same as the passive tracer, as expected. Our study suggests that passive tracers seem to be more important than temperature anomaly in the extratropics, but not in the equatorial region. If we decompose a thermocline temperature anomaly into the salinity-compensated component and the dynamically active component, the former may be more important in the extratropics, while the latter more important for the equatorial region.

Our study here, although idealized, may have implications for recent studies of the Pacific decadal oscillation (PDO). It has been suggested that (Gu and Philander 1997; Zhang et al. 1998) the subduction from the midlatitude North Pacific into the equator may provide a critical time delay for the PDO. However, the PDO is also proposed to be mainly established by ocean–atmosphere interactions within the subtropical North Pacific (Latif and Barnett 1994; Barnett et al. 1999) with the equatorward subduction playing a passive role. With a simple ventilation thermocline model, Schneider et al. (1999) showed that the temperature anomaly subducted from the midlatitudes (Deser et al. 1996; Zhang and Liu 1999) is reduced rapidly before reaching the Tropics (about 20°N).

Our study suggests that the response of the equatorial thermocline to midlatitude forcing needs to be understood before a conclusion can be drawn on the role of equatorward subduction. The observed PDO constitutes the center of activity in the midlatitude North Pacific, which, according to our study, is likely to be the region that contributes the most to the equatorial thermocline on interdecadal timescales. The dominant PDO period is about 20 yr, which seems to be long enough to generate a detectable equatorial response. Of course, since the generated equatorial temperature anomaly is small compared with observation, positive ocean–atmosphere feedback is necessary for the extratropical buoyancy forcing to generate significant tropical climate response. The other implication is perhaps more relevant, yet subtle. Our understanding of the subduction of a temperature anomaly has been mostly limited to the subtropical region (Luyten et al. 1983; Liu 1999; Liu and Shin 1999; Schneider et al. 1999; Huang and Pedlosky 1999), where theory and observations seem to be consistent. In the Tropics, however, how a temperature anomaly penetrates into the equator has not been studied carefully. We have seen (Fig. 8 and Fig. 10) that the subduction propagation of a temperature anomaly in the Tropics differs dramatically from that in the subtropics. Once reaching the Tropics (at about 20°N), a temperature anomaly can reach the equator almost immediately (at least relative to a passive tracer), generating a submaximum there. This feature has not been reproduced in simple ventilation thermocline models, perhaps, due to the lack of the western boundary and some low-latitude dynamics. It should be pointed out that the final conclusion regarding the role of the equatorward subduction in PDO has to be tested in a fully coupled ocean–atmosphere model rather than an ocean-alone model. This is particularly true considering our results that the temperature in the Tropics and equatorial region respond to midlatitude forcing almost simultaneously. Therefore, even the observed local tropical wind (as was suggested by Schneider et al. 1999) may already be the consequence of the subduction anomaly that just reached the Tropics. Finally, the opposite sign response in the equatorial thermocline to the tropical buoyancy forcing may also be of interest to decadal climate variability because this response enables the off-equatorial buoyancy forcing to activate a negative delay in the thermocline.

Our study suggests that the regions of midlatitude mode water formation, such as North Pacific subtropical mode water and North Pacific central mode water (Yasuda and Hanawa 1997), may be the key regions where the midlatitude long-term buoyancy forcing affects the equatorial thermocline. This is so because the regions of mode water formation have deep mixed layers and therefore should result in a large local response. In the mean time, these midlatitude regions are also highly efficient in transmitting temperature anomalies into the equatorial thermocline through both subduction and wave propagation. Finally, our study suggests that the extratropical control on the equatorial thermocline may be even more important for understanding long-term climate changes such as global warming (e.g., Knutson and Manabe 1998) and the Last Glacial Maximum (CLIMAP 1981). This is so because these climate changes, with timescales longer than a century, should have the maximum EEP. In addition, these long term changes are usually accompanied by a broad surface pattern, which should also help to enhance the zonal mean local response and in turn the equatorial response.

Much further work is needed for a full understanding of the maintenance mechanism of the equatorial thermocline. The poor horizontal resolution is particularly worrisome, given that the LLWBC and coastal Kelvin waves seem to be of critical importance in transmitting the subtropical temperature signal into the equator. Realistic setting of ocean geometry and forcing are also needed to quantify observational issues. The effect of extratropical windstress should also be further studied beyond that of Liu and Philander (1995). Finally, the

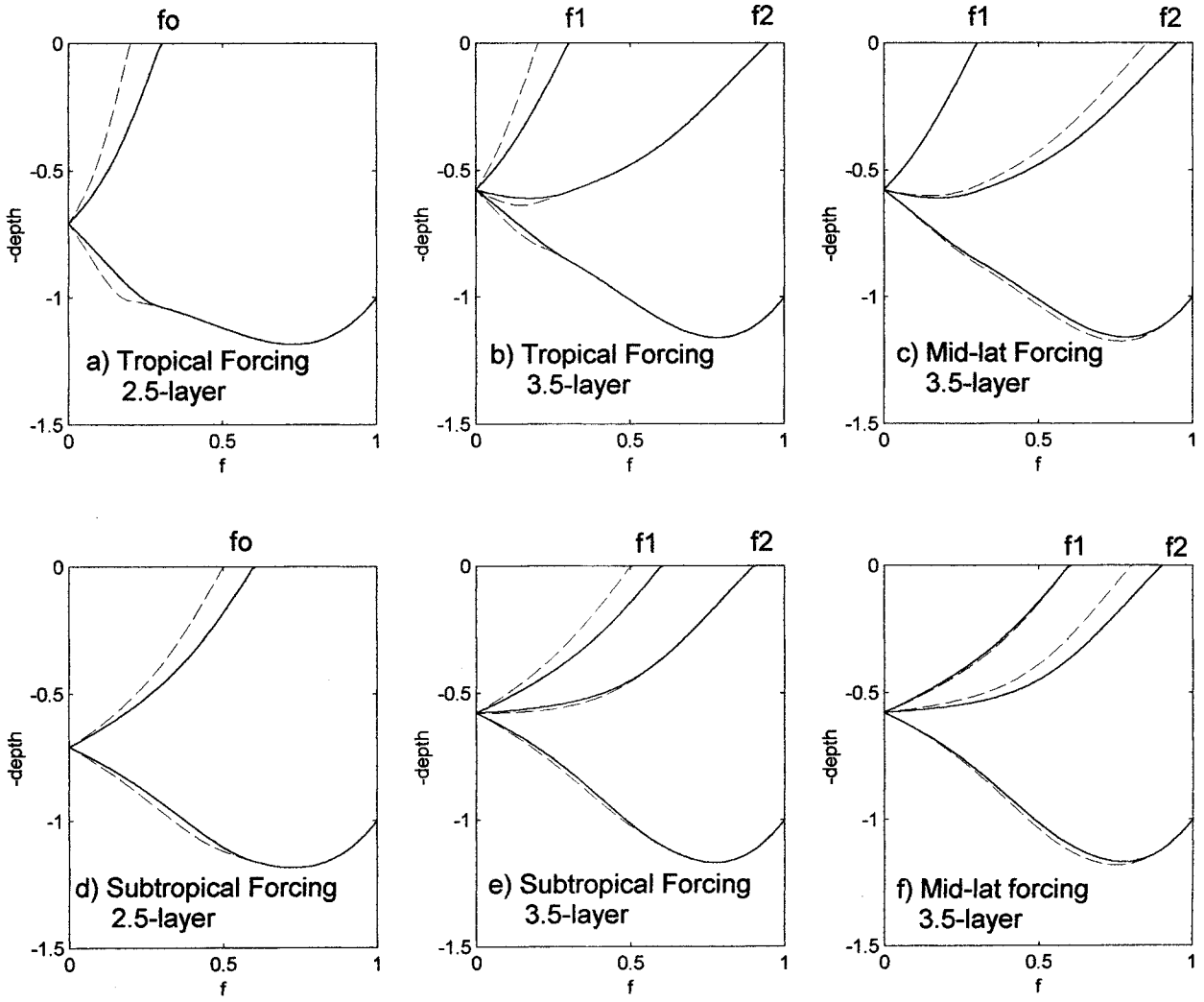

FIG. A1. Meridional profiles of ventilated zone thermocline solutions under the Ekman pumping profile $w_e(f) = -\sin(f\pi)$. Other parameters are $H = 1$ and $x/\beta\gamma = -1$. (a), (d) The 2.5-layer model thermocline solution [determined from Eqs. (A1) and (A2)]. The solids are forced by the outcrop line (a) $f_0 = 0.4$ and (d) $f_0 = 0.6$; the dashed lines are forced by a cooling perturbation such that $df_0 = -0.1$ in (a) the Tropics and (d) subtropics. (b), (c), (e), (f) The 3.5-layer solutions determined from Eqs. (A5). (b) and (c) Solid lines are for $f_1 = 0.4$ in the Tropics and $f_2 = 0.9$ in the midlatitude; the dashed lines are solutions by perturbation cooling $df_1 = -0.1$ in (b) and $df_2 = -0.1$ in (c); (e), (f) the same as (b) and (c), except for $f_1 = 0.6$ in the subtropics.

restoring surface forcing imposes a strong negative ocean–atmosphere feedback. Parallel experiments with anomalous flux forcing (Miller et al. 1994) may be useful to provide additional insights on the temperature response in the equatorial thermocline and surface.

Acknowledgments. We thank Dr. M. Hitchman for a helpful discussion and Ms. D. Lee for performing some experiments. We also thank Ms. M. Kennedy for editorial assistance. Comments from two reviewers have led to substantial improvements of the paper. This work is supported by NSF and NOAA.

APPENDIX

Response of the Ventilated Thermocline to Buoyancy Forcing

The distinct baroclinic structure of off-equatorial temperature response in the OGCMs can be understood in the ventilated thermocline model (Huang and Pedlosky 1999; Schneider et al. 1999). Although the ventilated thermocline model used here is not valid in the vicinity of the equator, it can still be used to infer many important features of equatorial responses, as demonstrated by Liu (1994) and Liu et al. (1994). In a 2.5-layer model, the ventilated zone interface depth of layer 2 (h) and layer 1 (h_1) are determined by the Sverdrup relation

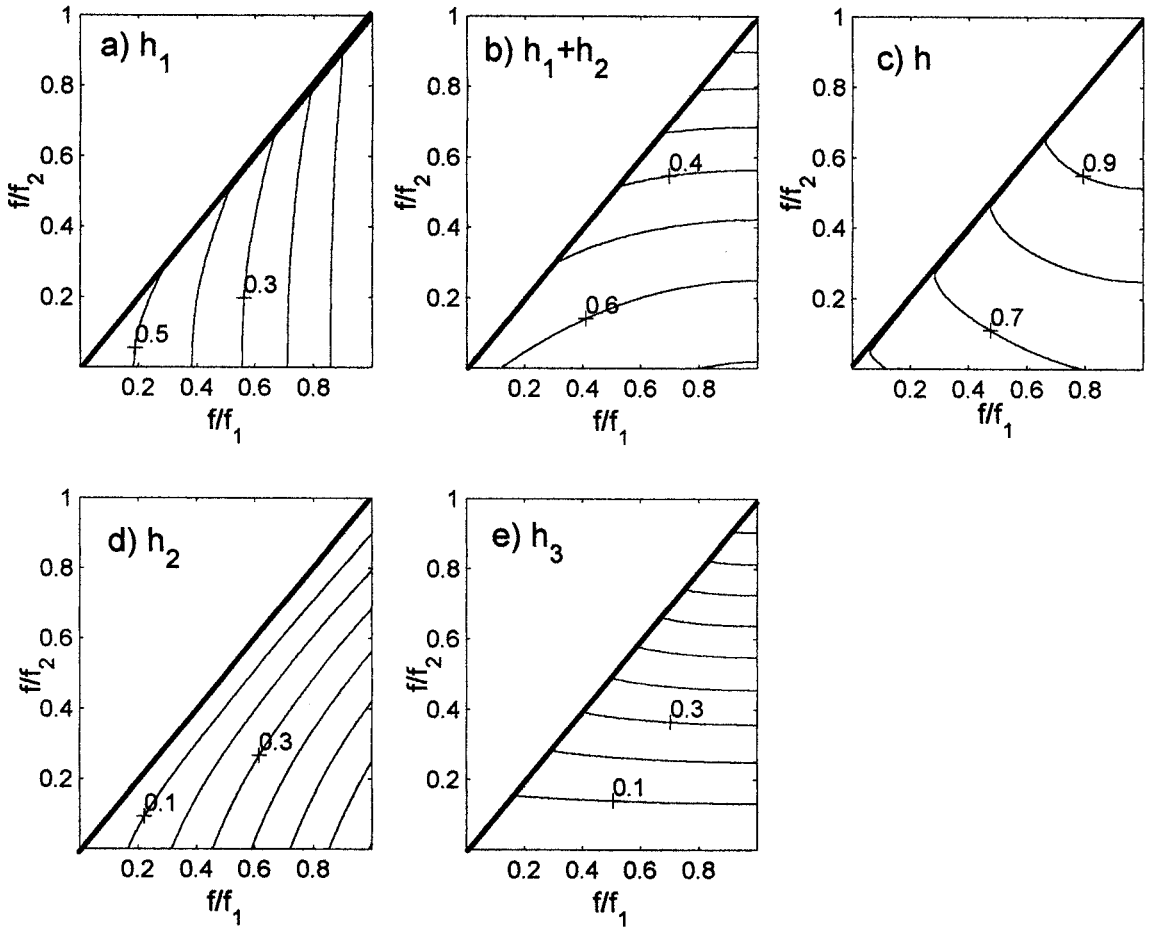

FIG. A2. Layer depths and thickness as a function of f/f_1 and f/f_2 for the 3.5-layer ventilated zone thermocline solution (A5) (setting $D^2 + H^2 = 1$); (a) layer 1 depth h_1, (b) layer 2 depth $h_1 + h_2$, (c) layer 3 depth h, (d) layer 2 thickness h_2, and (e) layer 3 thickness h_3.

$$h^2 + h_1^2 = D^2 + H^2, \tag{A1}$$

and the conservation of layer-2 potential vorticity (assuming a zonal outcrop line f_0)

$$f/(h - h_1) = f_0/h, \tag{A2}$$

Here H is a constant depth of h along the eastern boundary, $D^2 = -2f^2 w_e(f)x/\gamma\beta$ and γ is the reduced gravity across all the layer interfaces. The change of the layer interfaces with the outcrop latitude can be obtained from the differentiation of (A1) and (A2) with respect to f_0 as

$$dh_1^2/df_0 = -dh^2/df_0 = 2h_1^2/[f(1 + h_1)] > 0. \tag{A3}$$

Surface cooling ($df_0 < 0$) therefore results in a decrease in h_1 but an increase in h, corresponding to a second-modelike baroclinic response with upper thermocline cooling and lower thermocline warming. Two examples are shown in Figs. A1a and A1d, which are forced by tropical and subtropical forcing, respectively. Similar baroclinic responses have been discussed previously in OGCMs (Liu 1999; Liu and Shin 1999) and a ventilated thermocline model (Huang and Pedlosky 1999). It is important to point out here that the baroclinic response holds regardless of the shape of the outcrop line, because $dh_1^2/df_0 = -dh^2/df_0$ is derived from the Sverdrup relation (A1) alone.

The magnitude of the baroclinic response can also be studied. We can derive from (A3) and (A2) that

$$0 > \frac{\dfrac{dh}{df_0}}{\dfrac{dh_1}{df_0}} = -\frac{h_1}{h} = \frac{1}{1 - \dfrac{f}{f_0}} > -1. \tag{A4}$$

With a perturbation cooling ($df_0 < 0$), the warming magnitude in the lower thermocline ($dh > 0$) is always smaller than the cooling in the upper thermocline ($dh_1 < 0$). This feature can be seen in the examples of ventilated thermocline (Figs. A1a,d) and the OGCM (Fig. 4, Fig. 13). Furthermore, (A4) shows that, at a given low latitude f, the lower-thermocline warming increases for an outcrop line closer to the equator $f_0 \to f$. The

implication is that tropical surface cooling generates a much stronger lower thermocline warming than subtropical or midlatitude cooling. This is consistent with the examples in the ventilated thermocline and OGCM. The tropical cooling cases (Fig. A1a, Fig. 13a) generate much stronger thermocline warming than the corresponding subtropical and midlatitude forcing cases (Fig. A1d, Fig. 13c).

The baroclinic responses can be further understood in a 3.5-layer model. Following Luyten et al. [1983, their Eqs. (2.30) and (2.31)], the layer thickness in the ventilated thermocline zone are determined by

$$h^2 = (D^2 + H^2)/F, \qquad h_3 = \frac{hf}{f_2}, \qquad h_1 = h - h_2 - h_3,$$

$$h_2 = h\left(2 - \frac{f}{f_2}\right)\left(\frac{f}{f_1} - \frac{f}{f_2}\right)\Bigg/\left(2 - \frac{f_1}{f_2}\right), \tag{A5}$$

where $F = 1 + (1 - f/f_2)^2 + [1 - f/f_2 - (2 - f/f_2)(f/f_2 - f/f_2)/(2 - f_1/f_2)]^2$, f_1, and f_2 are the zonal outcrop lines for layer 1 and layer 2, respectively, and the reduced gravity is assumed the same across all layer interfaces. Two examples are presented with perturbation cooling on f_1 which is located in the Tropics (Fig. A1b) and subtropics (Figs. A1e). In both cases, the depth decrease for layer 1 but increase for layers 2 and 3, again corresponding to a second-modelike response with upper thermocline cooling and lower thermocline warming. In another two examples, the anomalous cooling acts on f_2 in the midlatitude (Figs. A1c,f). The resulted thermocline depths shallow for layer 2, but increase slightly for layer 1 and layer 3. This represents a strong subduction cooling in the midthermocline sandwiched by weak warming in the surface and lower thermocline, corresponding to a third-modelike response. This third-modelike response has been seen in the MICOM response to a midlatitude cooling (Figs. 13c,e). Furthermore, the middle and lower thermocline warming in the low latitude is the strongest under the tropical cooling forcing (Fig. A1b), also similar to the 2.5-layer case (Fig. A1a).

The baroclinic responses in Figs. A1b,c,e,f can be proven unchanged qualitatively in a general 3.5-layer model. This can be inferred from Fig. A2, in which layer depths and thickness are plotted against the two outcrop lines (in f/f_1 and f/f_2) for $f_2 > f_1$. A surface cooling on f_1 (increasing f/f_1 and fixing f/f_2) reduces the depth of the first layer (h_1) significantly (Fig. A2a), but increases the depths of both the second layer ($h_1 + h_2$) (Fig. A2b) and the third layer h (Fig. A2c) slightly, corresponding to a second-modelike structure as seen in Figs. A1b,e. As a result, layer thickness increase significantly for the second layer (h_2) (Fig. A2d) and slightly for the third layer (h_3) (Fig. A2e). In contrast, surface cooling on f_2 (increasing f/f_2 and fixing f/f_1) shoals the depth of layer 2 significantly (Fig. A2b), but deepens the depths of layer 1 slightly (Fig. A2a) and layer 3 modestly (Fig. A2c), corresponding to a third-modelike structure as seen in Figs. A1c,f. In turn, the layer thickness are reduced modestly in layer 2 (Fig. A2d) but increased significantly in layer 3 (Fig. A2e).

REFERENCES

Barnett, T, D. W. Pierce, M. Latif, D. Dommenget, and R. Saravanan, 1999: Interdecadal interactions between the tropics and midlatitudes in the Pacific basin. *Geophys. Res. Lett.,* **26,** 615–618.

Bleck, R., C. Rooth, D. Hu, and L. T. Smith, 1992: Salinity-driven thermocline transients in a wind- and thermohaline-forced isopycnal coordinate mode of the North Atlantic. *J. Phys. Oceanogr.,* **22,** 1486–1505.

Cane, M. A., A. C. Clement, A. Kaplan, Y. Kushnir, D. Pozdnyakov, R. Seager, and S. Zebiak, 1997: Twentieth century sea surface temperature trends. *Science,* **275,** 957–960.

CLIMAP Project Members, 1981: Seasonal reconstructions of the earth's surface at the Last Glacial Maximum. Geological Society of America Map Chart Series, Vol. 36.

Deser, C., M. A. Alexander, and M. S. Timlin, 1996: Upper-ocean thermal variations in the North Pacific during 1970–1991. *J. Climate,* **9,** 1840–1855.

Dewar, W., 1998: On ''too-fast'' baroclinic planetary waves in the general circulation. *J. Phys. Oceanogr.,* **28,** 1739–1758.

Fine, R. A., W. H. Peterson, and H. G. Ostland, 1987: The penetration of tritium into the tropical Pacific. *J. Phys. Oceanogr.,* **17,** 553–564.

Frankignoul, C., and P. Muller, 1979: On the generation of geostrophic eddies by surface buoyancy flux anomalies. *J. Phys. Oceanogr.,* **9,** 1207–1213.

Gent, P. R., J. Willebrand, T. McDougall, and J. C. Mcwillaims, 1995: Parameterizing eddy induced tracer transports in ocean circulation model. *J. Phys. Oceanogr.,* **25,** 467–474.

Gu, D., and S. G. H. Philander, 1997: Interdecadal climate fluctuations that depend on exchanges between the tropics and extratropics. *Science,* **275,** 805–807.

Haney, R. L., 1973: Surface thermal boundary condition for ocean circulation models. *J. Phys. Oceanogr.,* **3,** 241–248.

Hellerman, S., and M. Rosenstein, 1983: Normal monthly wind stress over the world ocean with error estimates. *J. Phys. Oceanogr.,* **13,** 1093–1104.

Hsieh, W. W., M. K. Davey, and R. C. Wajsowicz, 1983: The free Kelvin wave in finite-difference numerical models. *J. Phys. Oceanogr.,* **13,** 1383–1397.

Huang, R. X., and J. Pedlosky, 1999: Climate variability inferred from a layered model of the ventilated thermocline. *J. Phys. Oceanogr.,* **29,** 779–790.

Jenkins, W. J., 1991: Determination of isopycnal diffusivity in the Sargasso Sea. *J. Phys. Oceanogr.,* **21,** 1058–1061.

Killworth, P. D., D. B. Chelton, and R. A. de Szoeke, 1997: The speed of observed and theoretical long extratropical planetary waves. *J. Phys. Oceanogr.,* **27,** 1946–1966.

Knutson, T., and S. Manabe, 1998: Model assesment of decadal variability and trends in the tropical Pacific Ocean. *J. Climate,* **11,** 2273–2296.

Latif, M., and T. P. Barnett, 1994: Causes of decadal variability over the North Pacific and North America. *Science,* **266,** 634–637.

Levitus, S., and T. P. Boyer, 1994: *World Ocean Atlas.* Vol. 4: *Temperature. NOAA Atlas NESDIS 4,* U.S. Govt. Printing Office, Washington, DC, 117 pp.

——, R. Burgett, and T. P. Boyer, 1994: *World Ocean Atlas.* Vol. 3: *Salinity. NOAA Atlas NESDIS 3,* U.S. Govt. Printing Office, Washington, DC, 99 pp.

Liu, Z., 1993: Thermocline forced by varying wind. Part II: Annual and decadal Ekman pumping. J. *Phys. Oceanogr.,* **23,** 2523–2541.

——, 1994: A simple model of the mass exchange between the subtropical and tropical ocean. *J. Phys. Oceanogr.,* **24,** 1153–1165.

——, 1999: Forced planetary wave response in a thermocline gyre. *J. Phys. Oceanogr.,* **29,** 1036–1055.
——, and J. Pedlosky, 1994: Thermocline forced by annual and decadal surface temperature variation. *J. Phys. Oceanogr.,* **24,** 587–608.
——, and G. Philander, 1995: How different wind patterns affect the tropical–subtropical thermocline circulation in the upper ocean. *J. Phys. Oceanogr.,* **25,** 449–462.
——, and S. Shin, 1999: On thermocline ventilation of active and passive tracers. *Geophys. Res. Lett.,* **26,** 357–360.
——, G. Philander, and R. Pacanowski, 1994: A GCM study of tropical–subtropical upper ocean mass exchange. *J. Phys. Oceanogr.,* **24,** 2606–2623.
——, L. Wu, and E. Bayler, 1999: Rossby wave–coastal Kelvin wave interaction in the extratropics. Part I: Low frequency adjustment in a closed basin. *J. Phys. Oceanogr.,* **29,** 2383–2404.
Luyten, J., J. Pedlosky, and H. Stommel, 1983: The ventilated thermocline. *J. Phys. Oceanogr.,* **13,** 292–309.
Lysne, J., P. Chang, and B. Giese, 1997: Impact of the extratropical Pacific on equatorial variability. *Geophys. Res. Lett.,* **24,** 2589–2592.
Magaard, L., 1977: On the generation of baroclinic Rossby waves in the ocean by meteorological forces. *J. Phys. Oceanogr.,* **7,** 359–364.
McCreary, J., and P. Lu, 1994: On the interaction between the subtropical and the equatorial oceans: The subtropical cell. *J. Phys. Oceanogr.,* **24,** 466–497.
Miller, A., D. Cayan, T. Barnett, N. Graham, and J. Oberhuber, 1994: Interdecadal variability of the Pacific Ocean: Model response to observed heat flux and wind stress anomalies. *Climate Dyn.,* **9,** 287–302.
——, ——, and W. White, 1998: A westward-intensified decadal change in the North Pacific thermocline and gyre-scale circulation. *J. Climate,* **11,** 3112–3127.
Pacanowski, R. C., 1996: MOM2 documentation. GFDL Ocean Tech. Rep. 3.2, 329 pp. [Available from GFDL, P.O. Box 308, Princeton, NJ 08542-0308.]
Polzin, K., J. M. Toole, J. R. Ledwell, and R. W. Schmitt, 1997: Spatial variability of turbulent mixing in the abyssal ocean. *Science,* **276,** 93–96.
Schmitt, R. W., 1999: Spice and the Demon. *Science,* **283,** 498–499.
Schneider, N., A. J. Miller, M. A. Alexander, and C. Deser, 1999: Subduction of decadal North Pacific temperature anomalies: Observations and dynamics. *J. Phys. Oceanogr.,* **29,** 1056–1070.
Yasuda, T., and K. Hanawa, 1997: Decadal changes in the mode waters in the midlatitude North Pacific. *J. Phys. Oceanogr.,* **27,** 858–870.
Zhang, R. H., and Z. Liu, 1999: Decadal thermocline variability in the North Pacific: Two pathways around the subtropical gyre. *J. Climate,* **12,** 3273–3296.
——, L. M. Rothstein, and A. I. Busalacchi, 1998: Origin of upper ocean warming and El Niño change on decadal scales in the tropical Pacific Ocean. *Nature,* **391,** 879–883.